# Biosynthesis of Au–CuO–ZnO Nanocomposite using leaf extract and activity as anti- bacterial, anti-cancer, degradation of CB dye

**Luma Hakim Ali**
The General Directorate of Education in Babil province
**Wisam Aqeel Muslim**
The General Directorate of Education in Diwaniyah province
**Azhar Abees Ghali**
University of Al-Qadisiyah
**Karrar hazim Salem**
Al-Mustaqbal University College
**Kahtan A. Mohammed** ( kahtan444@gmail.com )
Hilla University College
**Rahman S. Zabibah**
the Islamic University
**Mohammed Ayad Alkhafaji**
National University of Science and Technology
**Manikandan Elayaperumal**
Government Arts and Science College, Thiruvalluvar University
**Noha Inam Ameen**
Goa University
**Kuldeep K. Saxena**
Lovely Professional University

**Research Article**

**Keywords:** Biosynthesis, anti-cancer, Au-CuO-ZnO, photodegradation, anti-bacterial, Wastewater

**Posted Date:** February 17th, 2023

**DOI:** https://doi.org/10.21203/rs.3.rs-2588002/v1

# Abstract

The photocatalytic degradation of Cibacron Brilliant Yellow 3G-P (CB) dye in aqueous solution using ZnO, CuO, Au–ZnO, Cu-ZnO, and Au–CuO–ZnO nanomaterials produced using *Acacia dealbata* leaf extract is described in this study. X-ray diffraction (XRD), Field emission- scanning electron microscopy (FE-SEM), transmission electron microscopic studies (TEM), atomic force microscopy (AFM), element analysis EDX, and diffuse reflectance UV-visible spectroscopy were used to characterize the structural, chemical, morphological, topological, and optical properties of as- synthesized nanomaterials, The characterization research validated the successful synthesis route and demonstrated the effective dispersion of Au and CuO over the ZnO surface. Furthermore, the XRD patterns were discovered to conform to the hexagonal structure of ZnO wurtzite. In addition, A hybrid Au-CuO-ZnO nanocomposite's compositional characterization was explored using EDX-mapping, which proved the efficient distribution of Zn, Cu, O, and Au in the hybrid composite. The roughness of the produced nanostructures was confirmed by topological analysis. With the doping of Au and CuO NPs, the absorption threshold edge of ZnO was moved from the UV to the visible area, according to the optical investigation. Under visible light irradiation, photocatalytic (CB) dye degradation studies demonstrated that the Au–CuO–ZnO nanocomposite is more efficient than pure ZnO at degrading the dye. After 50 minutes After 45 minutes of illumination under ideal circumstances of 1.0 g/L photocatalyst, 10 ppm (CB) dye, and pH 10, photodegradation efficiency of up to 99 percent was achieved. Photogenerated holes and hydroxyl radicals are responsible for the increased photodegradation efficiency of Au–CuO–ZnO, according to the reactive species investigation. The Au-CuO-ZnO nanocomposite displayed high potential stability and recyclability, with 78.6 percent photoactivity remaining after five cycles, according to the recycling data. and study the effect of Au-CuO-ZnO nanocomposite on bacteria of coli Escherichia and Staphylococcus aureus, where these bacteria were used as a representative of the cream negative bacteria and the positive bacteria respectively. The results showed the rate of success (Au-CuO-ZnO nanocomposite) in eliminating and destroying these bacteria and this is possible by using the nanoscale solution to sterilize and eliminate bacteria. By assessing cytotoxicity, it was demonstrated that Au-CuO-ZnO nanocomposite can both kill and stop the proliferation of cancer cells. When compared to cancer cells not treated with the chemical, the Au-CuO-ZnO nanocomposite shown very deadly efficiency against cancer cells by preventing their development and reproduction. One of the most crucial techniques for identifying inhibition in living cells is the procedure of determining the toxicity of the synthesized chemicals. Au-CuO-ZnO nanocomposite had a biological activity with an IC50 of 35.33 g/ml.


# Introduction

Industrial wastewaters are now exceedingly harmful to aquatic ecosystems, humans, and other creatures because they constitute a severe threat to the natural environment. However, because of the continued increase in pollution sources and an expanding population, it remains the world's most serious concern [1]. Certainly, as industrial operations expand, so does the need for water, and as a result, large amounts of wastewater effluent are frequently released into clean water sources, causing serious environmental

issues. Intensive effluents of dyes, paints, heavy metal ions and detergents are responsible for the majority of water hydrocarbons, phenolic compounds, Petrochemicals, pesticides, plastics, pharmaceuticals, fertilizers, and dairy quality concerns. Due to their anomalous physical and chemical features, these polluted water compounds are extremely complex and hazardous [2]. The rising pollution of water bodies by colored effluents is currently one of the most dangerous environmental challenges, Damage to the aquatic environment and various diseases in animals and humans are common problems associated with textile dyes' environmental contamination, which is caused by increasing chemical and biochemical oxygen demand (COD and BOD), reducing photosynthesis, inhibiting plant growth, and accumulating through the aquatic food chain [3]. One of the most effective methods for wastewater treatment is photocatalysis, which, in comparison to other technologies, provides advantages such as quick and nearly total elimination of wastewater pollutants and the absence of harmful intermediates and byproducts Because of its significant potential for full mineralization of numerous nonbiodegradable organic contaminants in the aqueous media, photocatalysis is an established technology for removing various pollutants in wastewaters [4, 5]. Due to its remarkable physical and chemical properties, zinc oxide (ZnO) is one of the most researched photocatalysts. ZnO is a widely used n-type oxide semiconductor with a band gap energy (Eg) of 3.35 eV. It was discovered that the ZnO band energy value varies between 3.1 and 3.4 eV. As a result, the band gap of ZnO has been discovered to be sensitive to the synthesis technique as well as the size and form of its crystals [6]. Due to its fast oxidation potential, stability against biological and chemical interactions, strong redox ability, nontoxicity, cheap cost, and environmental safety, ZnO appears to be superior to the rest of the materials, Biosensing, adsorption, solar cells, photocatalysis, medicinal and biological applications are only a few of the sectors where ZnO is becoming more relevant [7]. Furthermore, electron-hole pairs can only be generated primarily by high-energy UV photons due to their optical wide-band-gap energy. Although bare ZnO is often not photoing catalytically active in visible light, it may respond to the action of solar radiation, in specific conditions, such as self-sensitization, and vacuum deoxidation, ZnO has been subjected to modification procedures such as surface reduction of metals such as Ag, Fe, Au, Pd, and Cu to overcome its photocatalytic restriction because to its large band gap energy [8]. Au and other noble metal nanoparticles have been shown to boost visible light absorption and charge separation in oxide semiconductors, improving photocatalytic efficacy. Another successful technique to change the bandgap of ZnO nanohybrid materials is to combine it with narrow bands of gap oxide semiconductors such as CuO, $Fe_2O_3$, and $Ag_2O$ [9]. Other techniques, including plasma treatment, dye sensitization, and heat treatment, can be used to modify the optical band gap of ZnO. As a result, the presence of narrow band gap oxide semiconductors and/or metals in ZnO nanostructures might potentially expand the spectrum sensitivity to visible light [10]. CuO has a narrower band gap (1.2 eV) than ZnO, therefore combining CuO NPs with ZnO NPs should improve photoelectron transfer due to more effective charge-carrier separation and acceptable band locations, and so the $Cu_2^+$ ions have affected the band structure of ZnO, it was discovered that injecting photogenerated electrons from CuO into ZnO increased photocatalytic activity. in water splitting, photodegradation of organic dyes and dye-sensitized solar cells [11]. In recent years, there have been a few publications in the literature regarding generating the ternary nanocomposite Au–CuO–ZnO using various regular synthetic procedures. However, these procedures have several drawbacks, the likelihood

of harmful physical therapies or medicines, excessive energy use, and high expense. A global drive toward a more environmentally friendly nanocatalyst production technique has recently gained momentum. Environmentally friendly processes have been employed to biosynthesize ZnO NPs from plant extracts, bacteria, fungi, and algae [12]. Plant extracts such as roots, flowers, leaves, stems, seeds, and fruits, have been reported to be used to make ZnO NPs. Green synthesis of ZnO NPs, on the other hand, allows for large-scale manufacturing with fewer unwanted contaminants. For the examination of photocatalytic degradation of Cibacron Brilliant Yellow 3G-P (CB) dye under visible light irradiation, binary Cu–ZnO and ternary Au–CuO–ZnO nanocomposites were made utilizing *Acacia dealbata* leaf extract as a simple and low-cost green route. There are just a few articles on the green synthesis of ternary hybrid Au-CuO-ZnO nanocomposites utilizing plant extracts that we are aware of. Techniques The nanomaterials were examined using techniques such atomic force microscopy (AFM), X-ray diffraction (XRD), scanning electron microscopy (FE-SEM), energy-dispersive X-ray spectroscopy (EDX), and transmission electron microscopy (TEM). explore the impact of Au-CuO-ZnO nanocomposite on Staphylococcus aureus and coli Escherichia bacteria, which were utilized as examples of cream positive and cream negative bacteria, respectively. According to the data, Au-CuO-ZnO nanocomposite has a high rate of success in eradicating and destroying harmful germs. This success rate demonstrates how useful nanoscale solutions are for sterilizing wounds and getting rid of bacteria. By assessing cytotoxicity, it was demonstrated that Au-CuO-ZnO nanocomposite has the power to destroy cancer cells and stop their proliferation. In contrast to untreated cancer cells, the Au-CuO-ZnO nanocomposite demonstrated great lethal efficacy against cancer cells by preventing their development and proliferation. One of the most crucial approaches for identifying inhibition in living cells is the procedure of assessing the toxicity of the synthesized chemicals. Au-CuO-ZnO nanocomposite had an IC50 of 35.33 g/ml for biological activity.

# Experimental Details

## Materials

All materials supplied are analytical reagent grade and may be used right away. Sigma-Aldrich provided the zinc (II) nitrate hexahydrate (Zn $(NO_3)_2.6H_2O$, 99 percent), hydrogen tetrachlorocuprate (III) hydrate ($HAuCl_4$ $3H_2O$), cupric acetate monohydrate $(CH_3COO)_2Cu.H_2O$, 99.0%), and 99 percent Cibacron Brilliant Yellow 3G-P dye (99%), F.wt = 872.97 λmax = 404 nm, Scharlau supplied 99.5 percent ethanol ($C_2H_5OH$), 37 percent hydrochloric acid (HCl), and 99 percent sodium hydroxide (NaOH). Deionized water was used to make all the solutions (DW).

## Catalysts characterization

Cu K irradiation using a Ni-filtered Shimadzu XRD 6000 diffractometer (=1.54056) at temperatures between 20° and 80° were used to determine the crystal phase of nanomaterials as they had been manufactured. Field emission-scanning electron microscopy (FE-SEM) and transmission electron microscopy (TEM, Hitachi H-9500) were used to analyze the morphology and size of nanomaterials as they were produced (FE-SEM, MIRA3 TESCAN, Czech). Functional groups and molecular structures of as-

prepared nanomaterials were determined using energy dispersive X-ray spectroscopy (EDX) in conjunction with a scanning electron microscope (SEM). We were able to calculate the surface elemental composition of the nanomaterials as a result. Atomic force microscopy (AFM) techniques were used to investigate as-fabricated nanomaterial. Shimadzu-PC Japan's 1650 UV-Visible spectrophotometer was used to track the photodegradation of the Cibacron Brilliant Yellow 3G-P (CB) dye by measuring its maximum absorption band (max = 404 nm).

### Preparation of aqueous extract using Acacia dealbata leaf

Fresh *Acacia dealbata* leaves were taken from an open field in Babil, Iraq, and cleaned completely with deionized water (DW). Then it was placed in a dust-free environment overnight to prevent volatile organic chemicals from evaporating. The leaves were then cut and put in 75 mL of DW, where they were heated for 30 minutes at 800°C with vigorous stirring. The extract was then filtered using Whatman No.1 filter paper and centrifuged for 15 minutes at 6000 rpm to remove tiny suspended particles. By adding DI water to the final amount, it was brought to 100 mL. The clear extract was then kept at 40 degrees Celsius for use in nanomaterial production.

### Synthesis of ZnO, CuO and Au nanoparticles using Acacia dealbata leaf extract

There was only ZnO nanoparticle synthesis done. The usual procedure was to dissolve Zn (NO3)2.6H2O (0.01 M) in 50 mL of aqueous Acacia dealbata extract, and then to reduce it to Zn2+ ions by magnetic stirring continuously for 4 hours at 800C. After that, a substantial piece of metal foil was placed over the solution to shield it from any photo reactions and it was left at room temperature for 24 hours. For 20 minutes, the reaction mixture was centrifuged at 6000 rpm. The brown precipitate was repeatedly washed with DW and ethanol DW, and any adsorptive impurities were then removed by drying the mixture at 800C for four hours. This solid was then produced. The white solid that was produced is evidence of ZnO NPs formation. The solid was calcined at 500°C after that 4 h. In a separate experiment, Zn $(NO_3)_2.6H_2O$ was dissolved in deionized water (without Hibiscus Sabdariffa extract) and the same stages as the preceding approach were followed, but no ZnO precipitate was generated under the circumstances described above. CuO NPs were prepared using the same process as previously, except for dissolving $(CH_3COO)_2Cu.H_2O$ (0.01 M) into aqueous *Acacia dealbata* extract, which resulted in a black colored CuO NPs. Au NPs were prepared using the same process as previously, except that 0.5 g of Hydrogen tetrachlorocuprate (III) hydrate ($HAuCl_4$. $3H_2O$ 99.9%) was dissolved in aqueous Citrus medica extract, resulting in leaning to yellow colored Au NPs after the heating process, the same technique was used this time.

### Synthesis of CuO-ZnO and Au-ZnO nanocomposite by Acacia dealbata leaf extract

CuO-ZnO nanocomposite has been created with a molar ratio of 1:9. In one experiment, 4.09 g/L Zn $(NO_3)_2.6H_2O$ and 0.51 g of $(CH_3COO)_2Cu.H_2O$ was dissolved in 50 mL of aqueous *Acacia dealbata* extract, then 4 hours of continuous magnetic stirring at 800C were performed. In order to prevent photo reactions, the solution was then covered with a thick metal foil and left at room temperature for 24 hours. The reaction mixture was centrifuged at 6,000 rpm for 20 minutes. The resultant precipitate was then

repeatedly washed with DI and ethanol to get rid of any adsorptive impurities before being dried at 80°C for four hours to get a light blue solid. After that, the gray-colored powder was calcined for 4 hours at 500°C. Au-ZnO nanocomposite was prepared using the same process as previously, except that 0.19 g/L Hydrogen tetrachlorocuprate (III) hydrate ($HAuCl_4$. $3H_2O$ 99.9%), was dissolved in aqueous Citrus medica extract, resulting in leaning to yellow colored Au NPs after the heating process.

### Synthesis of Au-CuO-ZnO nanocomposite by Acacia dealbata leaf extract

Au-CuO-ZnO nanocomposites were synthesized in a 0.5:0.5:10 molar ratios. In a typical, Zn $(NO_3)_2.6H_2O$ (0.01M), $CH_3COO)_2Cu.H_2O$ (0.0005 M) and Hydrogen tetrachlorocuprate (III) hydrate ($HAuCl_4$. $3H_2O$ 99.9%), (0.0005 M) were dissolved into 50 mL of aqueous *Acacia dealbata* leaf extract followed by continuous magnetic stirring at 800C for about 4 hours. Then, to prevent any photo interactions, the solution was wrapped in thick aluminum foil and left at room temperature for 24 hours. Centrifuged for 20 minutes at 6000 rpm was the reaction mixture. The resulting precipitate was repeatedly cleaned with DW and ethanol to get rid of any adsorptive impurities before being dried at 800C for 4 hours to yield a light blue solid. The obtained gray-colored solid was then obtained after calcination at 500°C for 4 h.

### Photocatalytic degradation of Cibacron Brilliant Yellow 3G-P dye

The photocatalytic activity of as-produced nanomaterials was tested utilizing a handmade photoreactor as an enclosed chamber to degrade Cibacron Brilliant Yellow 3G-P (CB)dye in an aqueous solution under visible light irradiation. The photoreactor has a 200 W Xenon lamp as a visible light source and a temperature controller. The bulb was positioned 10 cm above the reaction mixture in the reactor's middle. A beaker containing 25 mL of (CB) dye solution and a particular amount of photocatalyst was then continuously stirred for 60 minutes in the dark to establish the adsorption/desorption equilibrium of the dye molecules on the catalyst's surface. Every time you run, before irradiating the dye solution, the lamp was switched on for 5 minutes to warm up. Following that, the zero-time reading was taken at the time when the dye solution was irradiated with lamp light, and the suspension was exposed to visible light for 120 minutes while being magnetically stirred and thermostatic at a constant temperature. At predetermined intervals, 1 mL suspension samples were taken, centrifuged at 6000 rpm to remove all catalyst particles, and the supernatant was collected to measure the residual dye concentration by measuring its absorbance at 404 nm. Changes in absorption peaks at 404 nm were used to compute (CB)dye photo decolorization efficiency (PDE percent). The following equation was used to compute the photo decolorization effectiveness (percentage):

$$\mathrm{PDE\%} = \frac{A_0 - A}{A} \times 100 \qquad 1$$

Ao and A, respectively, represent the absorbance of the (CB) dye at t = 0 and t = 1. No dye photo decolonization took place under these conditions, according to blank experiments in (CB) dye solution without a photocatalyst. Except as otherwise noted, all runs were performed in identical

settings. Numerous operational factors, including catalyst dose (0.4–1.4 g/L), pH (2–10), and beginning dye concentration (5–25 ppm), have been investigated for their effects on degrading effectiveness.

### Effect of Radical Scavengers

Several active radical species, including hydroxyl radicals ($^{\bullet}OH$), superoxide radicals ($^{\bullet}O_2$), and holes ($h^+$), are involved in the photocatalytic destruction of dyes. The scavengers used during the photodegradation of (CB) dye are potassium iodide (KI, a quencher of $^{\bullet}OH$ and $h^+$) [50], tert-butanol (TB, a quencher of $^{\bullet}OH$), and para-benzoquinone (BQ, a quencher of $^{\bullet}O_2$ scavenger) [51], respectively, to detect the roles of the reactive species generated during the photocatalytic reaction, 1.0 mM of each active species scavenger was introduced separately, and the same approach as in previous photocatalytic studies was followed.

### Reusability of Au-CuO-ZnO photocatalyst

For the Au-CuO ZnO nanocomposite, reusability tests were performed. The Au-CuO-ZnO NPs were separated using centrifugation at 800 rpm for 20 minutes after being utilized in the (CB)dye photodegradation procedure. The catalyst was subsequently utilized without purification in a second (CB)dye degradation test experiment. A total of five tests were conducted in a row. These tests were carried out similarly to the previous photocatalytic testing. Where the photodegradation rate in the first reuse was 99.4%, the rate of photodegradation after the second use reuse is 92.6%, and the rate of photodegradation after the third and fourth reuse is 87.9%, and 82.1 and the photodegradation rate after the last reuse is 78.6.

## Results And Discussion

### X-Ray Diffraction (XRD)

The XRD technique was used to examine the crystalline structures and diffraction patterns of produced nanomaterials in the 200-800 range. All XRD peaks of ZnO NPs have been meticulously catalogued as hexagonal wurtzite phase of ZnO (JCPDS card no. 24-1852) has angles 2Θ 31.4387° corresponding to 100 and 34.7359° corresponding to 002 and 36.2739° corresponding to 101 This indicates the formation of zinc oxide and Average nano Size 19.1321 nm and it matches previous studies [13]. as shown in Figure (1). Au NPs have a monoclinic XRD pattern, which indicates that Au is formed in single phases (JCPDS 78-1809). Au NPs have characteristic peaks centred at 38.2625°,44.3267°, and 64.1247°, which are ascribed to the lattice planes of Au NPs (111), (200), (220), and Average nano Size 31.8364 nm and it matches previous studies [14]. as shown in Figure (1). CuO NPs have a monoclinic XRD pattern, which indicates that CuO is formed in single phases (JCPDS 93-1236). CuO NPs have characteristic peaks centred at and 35.6851°, 38.7152°,48.6175°, which are ascribed to the lattice planes of CuO NPs (002), (111), (202), and Average nano Size 35.81 nm and Average nano Size 26.9588 nm and it matches previous studies [15]. Significant diffraction peaks correspond to the expected Au-ZnO in the XRD pattern of the Au-ZnO nanocomposite, which is compatible with the JCPDS cards of ZnO and Au NPs. Where the

large diffraction peaks of Au NPs appear to have angles of 2Θ 38.2625° corresponding to 111 and 44.2763° corresponding to 200 This indicates the formation of Au NPs, which indicates the growth of Au NPs on the surface of the zinc oxide nanoparticles, which indicates the formation of the Au-ZnO nanocomposite (90:10) and Average nano Size 29.0317 nm The structure of ZnO NPs is highly preserved after the inclusion of both Au nanoparticles, as-synthesized has an excellent crystalline structure. and it matches previous studies [16]. CuO-ZnO nanocomposites have unique peaks at 35.76° and 38.81° in their XRD pattern, which are indexed to the (002) and (200) of CuO, respectively. In addition, the combination of CuO and ZnO NPs resulted in decreased crystallite sizes and changed diffraction intensities. The structure of ZnO NPs is well retained with the addition of CuO and Au nanoparticles, as evidenced by the Au-CuO-ZnO nanocomposite's XRD pattern. In addition, a single weak peak for Au at 38.510 corresponding to (111) and a faint peak for CuO at 35.520 corresponding to (002) are visible, indicating that demonstrating that the produced ternary Au–CuO–ZnO nanocomposites have excellent crystalline structure The crystallite size of produced nanomaterials was calculated using the Debye-Scherer equation [17], and the results are reported in Table (1):

$$D = \frac{K\lambda}{\beta \times cos\theta} \qquad 2$$

The full width at half maximum (FWHM) of the XRD peaks, the diffraction angle, the crystallite size K, the wavelength of the X-ray beam (1.54), and the wavelength of the X-rays are all constants. According to XRD analysis, Table (1) displays the size of nanocrystallites in synthesized nanomaterials. The sample particle's size is nm.

| | ZnO | CuO | Au | CuO- ZnO | Au -ZnO | Au- CuO- ZnO |
|---|---|---|---|---|---|---|
| **2Θ** | 31.4387 | 35.6851 | 38.2625 | 31. 7672 | 32.6570 | 31. 4185 |
| | 34.7359 | 38.7152 | 44.3267 | 35.3897 | 34.4692 | 34.4320 |
| | 36.2739 | 48.6175 | 64.1247 | 36.1458 | 36.2387 | 36.9815 |
| **Average Size nm** | 19.1321 | 26.9588 | 31.8364 | 30. 1594 | 29.0317 | 35.9805 |

### Field-Emission Scanning Electron Microscopy (FE-SEM)

FE-SEM analysis was used to look at the surface morphologies of ZnO, CuO, and Au, as well as their nanocomposites. Figure (2) shows how nanostructures with porous surfaces develop in FE-SEM pictures. The FE-SEM micrographs demonstrated that ZnO NPs had a spherical, quasi-spherical, hexagonal, and rod-shaped structure, as well as being anisotropic in nature. When comparing biosynthesized CuO to ZnO NPs, FE-SEM examination revealed the synthesis of spherical-shaped nanoparticles with homogeneous particle shape and size and little aggregation [18]. The biosynthesized Au NPs have a quasi-spherical shape and a uniform distribution, as seen in the FE-SEM pictures [19]. The morphology of ZnO NPs

changes when CuO NPs are included, as revealed by FE-SEM analysis ,of As-synthesized CuO-ZnO nanocomposite is formed of quasi-spherical nanoparticles with agglomerated ZnO NPs that incorporated with spherical CuO NPs, resulting in a porous and rough surface, as seen by SEM micrographs. The FE-SEM pictures of the Au-ZnO nanocomposite revealed excellent dispersion of spherical Au NPs over the rough ZnO surface, as well as non-uniform distribution sizes and some aggregations [20]. Spherical particles may be detected on the CuO-ZnO NPs surface after Au NPs are doped, suggesting the creation of an Au–CuO–ZnO nanocomposite. As a result, the FE-SEM study proved that extremely porous nanostructures were synthesized. Energy Dispersive X-ray spectroscopy analysis was used to investigate the chemical composition and distribution of nanoparticles in the hybrid nanostructure. Figure (3) shows the EDX spectra of nanomaterials as-fabricated. The presence of Cu and O for CuO and Zn and O for ZnO is confirmed by EDX spectra, with no evidence of impurity peaks, indicating the presence of copper oxide and zinc oxide, respectively. EDX analysis also confirms that the Au sample is entirely made up of Au atoms. CuO-ZnO and Au-ZnO nanocomposites have EDX spectra that clearly show the presence of Cu, Zn, O and Au, Zn, O, respectively. The Au-CuO-ZnO nanocomposite has an identical elemental composition of Au atoms in addition to Zn, Cu, and O, according to EDX analysis. In addition, the EDX spectrum of the Au-CuO-ZnO sample shows that the Zn signal is strong, with the Au, Cu, and O peaks visible. The creation of metal oxides has been confirmed. Furthermore, EDX maps in Figure (4) reveal that the Au element has a uniform dispersion, but the Cu and O atoms are dispersed equally and uniformly across the ZnO surface. The uniform distribution of Cu, O, and Au on ZnO might result in a high number of effective heterojunction Au-CuO-ZnO contacts, enhancing the photocatalytic activity of Au-CuO-ZnO nanocomposite [21].

## Elemental of analysis (EDX)

The EDX spectra of nanomaterials as they are manufactured are shown in Figure (4). EDX spectra show no sign of impurity peaks and indicate the existence of Cu and O for CuO and Zn and O for ZnO, respectively, The Au sample's whole atomic composition is also confirmed by EDX analysis. The EDX spectra of Cu, Zn, O and Au, respectively are visible in the nanocomposites of CuO-ZnO and Au-ZnO. The Au, Cu, Zn and O peaks are readily discernible in the EDX spectrum of the Au-CuO-ZnO sample, which also reveals a strong Zn signal. Metal oxide synthesis has been shown. As for the Au-CuO-ZnO nanocomposite the Cu and O atoms are evenly distributed across the ZnO surface and the Au element exhibits a uniform dispersion. The Au-CuO-ZnO nanocomposite's photocatalytic activity may be increased by the uniform distribution of Cu, O, and Au on ZnO due to the potential for many heterojunction Au-CuO-ZnO connections [22].

Table (2): shows the ratios of each of the elements zinc, copper, Gold and oxygen

| Sample | Element | Weight% | Atomic% |
|---|---|---|---|
| ZnO | O | 31.06 | 82.98 |
| | Zn | 68.94 | 17.02 |
| Au | Au | 100 | 100 |
| CuO | O | 32.26 | 78.11 |
| | Cu | 67.74 | 21.89 |
| CuO- ZnO | O | 41.83 | 73.68 |
| | Zn | 48.47 | 19.22 |
| | Cu | 9.70 | 7.10 |
| Au- ZnO | O | 53.12 | 69.53 |
| | Zn | 35.48 | 23.35 |
| | Au | 11.4 | 7.12 |
| Au-CuO- ZnO | O | 50.33 | 55.79 |
| | Zn | 39.67 | 19.42 |
| | Au | 3.43 | 7.85 |
| | Cu | 6.57 | 16.94 |

### Transmission Electron Microscopy (TEM)

The morphologies and sizes of the nanomaterials as they were created were investigated further using the TEM method. Figure (5) shows TEM micrographs of all the manufactured nanomaterials used in this investigation, which may be used to explore particle shapes and sizes in more depth. The picture of ZnO NPs shows that the particles are generally spherical and hexagonal in form, with few agglomerations, supporting the FE-SEM study. The particle size ranged from 50 to 200 nanometers. The TEM picture of the produced CuO NPs revealed spherical CuO NPs with an average particle size of 25 nm, which is consistent with the FE-SEM results. The TEM micrograph of Au NPs demonstrates that they are virtually spherical, with individual particle mean diameters ranging from around the wavelength ranges between 20 and 84 nanometers. The excellent capping and stabilizing characteristics of *Acacia dealbata* leaf extract were confirmed by the uniformly dispersed Au NPs. The particle sizes appear to be larger with apparent agglomeration and non-uniform distribution of CuO and ZnO NPs in the TEM picture of CuO doped ZnO. The average size of Au-ZnO NPs was found to be in the range of 17-48 nm in TEM images of almost spherical-shaped agglomerated nanoparticles. All nanoparticles with diverse morphologies can be observed in the TEM picture of Au-CuO-ZnO nanocomposite. Furthermore, the anisotropic nanostructure of Au-CuO-ZnO is revealed by TEM micrographs, which show considerable agglomerations of nanoparticles [23,24].

## (AFM) Atomic Force Microscopy

The topographic characteristics of the as-synthesized nanomaterials were investigated using AFM analysis. Figure (6) shows a 3D and 2D picture of an Au-CuO-ZnO nanocomposite that was studied using an AFM in tapping mode. Table (3) summarizes the topographic features of nanomaterials as synthesized. The average roughness values (Ra) of ZnO, CuO, and Au NPs surfaces were 3.29, 2.17, and 7.11 nm, respectively, as shown in Table (3). Roughness increases to 24.9 and 26.8 nm after coupling with CuO NPs and doping with Au NPs, respectively. When compared to other ZnO nanostructures, the Au-CuO-ZnO nanocomposite has a bigger surface roughening (29.7 nm), indicating that this sample has a higher surface/volume ratio, which would promote electron-hole pair formation when light is applied to the surface [25]. ZnO, CuO, and Au NPs had thicknesses of 12.41, 10.0, and 12.63 nm, respectively, and Au-ZnO NPs have a thickness of 50.9 nm, with CuO-ZnO NPs having a thickness of 27.92 nm (108.2 nm) the Au-CuO-ZnO nanocomposite has a thickness 112.37. AFM research revealed a fluctuation in nanostructure thickness that is virtually identical to the grain size variation trend seen in Table (3). Agglomeration is enhanced as a result of the high concentration of sample NPs, increasing the thickness and surface roughness of ZnO nanocomposites. Furthermore, Table (3) shows that the higher roughness of as-produced nanomaterials surfaces is characterized by negative skewness (Rsk) values, suggesting a surface with more deep and severe valleys. Also, the kurtosis parameter (Rku) is a statistical measure used to describe the asymmetry and the flatness of the surface distribution. While Rku<3, all synthesized nanostructures could be described as spiky surfaces [26].

| Amplitude Factors | **ZnO** | **CuO** | **Au** | **Au - ZnO** | **CuO- ZnO** | **Au -CuO -ZnO** |
|---|---|---|---|---|---|---|
| Ra nm | 3.29 | 2.17 | 7.11 | 26.8 | 26.7 | 25.1 |
| Rq nm | 3.41 | 2.29 | 8.20 | 30.4 | 30.9 | 22.7 |
| Rsk nm | -0.0186 | 0.00572 | 0.0339 | -3.40 | -3.2 | -0.0142 |
| Rku nm | 1.52 | 1.69 | 1.3 | 1.95 | 1,91 | 2.41 |
| Thickness | 12.41 | 12.63 | 10,00 | 27.92 | 108.2 | 112.37 |

## Photocatalytic degradation of Cibacron Brilliant Yellow 3G-P dye

The dye solution Cibacron Brilliant Yellow 3G-P (CB) was utilized as a model for an organic environmental contaminant. In the absence of a photocatalyst, aqueous solutions of Cibacron Brilliant Yellow 3G-P (CB) dye were typically treated with visible light first, and the photodegradation efficiency was minimal. Figure (7) depicts the effect of irradiation duration on (CB) dye solution degradation efficiency in the presence of as-synthesized nanomaterials (1.0 g /L). As can be seen, the degrading efficiency of (CB) rose as the irradiation period increased. In comparison to other photocatalysts, however, the Au-CuO-ZnO nanocomposite illustrated in Figure (7) has the best photocatalytic efficiency. After 120 minutes of light irradiation, photodegradation of (CB) dye in the presence of Au-CuO-ZnO nanocomposite

reached 92.7 percent. Using bare ZnO as a photocatalyst resulted in the lowest (CB) dye photodegradation efficiency (51.3 percent) [27].

### Effect of photocatalyst dose

Au-CuO-ZnO concentrations ranging from 0.4 g/L to 1.4 g/L with fixation other settings [CB] = 20 ppm, pH = 7, irradiation period = 120 min, and T = 298 K were varied in a series of tests to find the optimal photocatalyst dosage and achieve efficient absorption of incident visible light. Increasing the photocatalyst dosage from 0.4 to 1.0 g/L, the photodegradation efficiency rose from 79.56 to 92.7 percent. More surface-active sites become accessible when the photocatalyst dosage is raised, enhancing the generation of more reactive radical species that drive the photodegradation process. A significant reduction in photodegradation efficiency was seen above the dosage of 1.0 g/L, which might be explained by the fact that excessive photocatalyst loading was used Excessive photocatalyst loading caused undesirable light scattering and the formation of impermeable suspension, As the photocatalyst dose rises, agglomeration owing to particle-particle interaction rises as well, which is a primary reason in the photocatalyst's decreased light absorption, For future research, a dose of 1.0 g/L Au-CuO-ZnO photocatalyst was used [28].

### Effect of initial dye concentration

The dye concentrations in wastewater effluents released from various stages of dyeing operations vary depending on the number of dyes employed in coloring processes. The amount of light that passes through the reaction solution to reach the photocatalyst surface is affected by the initial dye concentration. As a result, determining the influence of initial dye concentration on photodegradation efficiency is critical. The effect of dye (CB) concentration on photodegradation efficiency was investigated by increasing the starting dye concentration from 5 to 25 ppm while employing 1.0 g/L of catalyst at pH=7 and 298 K for 60 minutes under visible light irradiation Figure (9) shows. At a concentration of 5, the maximum photodegradation efficiency (99%) was achieved in a short irradiation duration. It has been discovered that when (CB) dye concentration grows, photodegradation efficiency decreases. This is because as dye concentration rises, more dye molecules become adsorbed on the surface-active sites, limiting photons' ability to reach the photocatalyst surface. As a result, raising the dye concentration reduces the availability of photoactive sites due to increased physical adsorption of dye molecules on the photocatalyst surface, resulting in decreased production of reactive species [29].

### Effect of initial pH

Because it regulates the surface charge of the catalyst, solution pH is one of the most important factors in heterogeneous photocatalytic processes. Figure (10) shows the influence of solution pH on the photodegradation effectiveness of Au-CuO-ZnO photocatalyst against Cibacron Brilliant Yellow 3G-P (CB) dye in the pH range of 2- 12. When the pH was elevated from 2 to 12 the photodegradation efficiency rose from 79.6% to 99.4%. The point of zero charges of Au-CuO-ZnO (pHzpc 8.43) as shown in Figure (10) might explain these observations. As a result, a shift in pH to an alkaline medium is predicted to

enhance the concentration of OH anions in the solution, resulting in more efficient production. OH radicals, the primary reactive oxygen species (ROS) that drive the photodegradation reaction are. OH, radicals in general. The formation of more $^{\bullet}OH$ from the $^{-}OH$ rather than $H_2O$ is mostly responsible for the increase in (CB) dye degradation efficiency in basic media, Due to functional protonation, the surface of Au-CuO-ZnO is positively charged at acidic pHs, competing with positively charged (CB) dye molecules for active site binding, resulting in decreased photodegradation efficiency. Above pHzpc, on the other hand, the photocatalyst surface is negatively charged due to saturation with hydroxyl anions, which promotes the adsorption of (CB) dye molecules via electrostatic attraction forces with the Au-CuO-ZnO surface, resulting in a considerable improvement in photodegradation efficiency [30].

## Kinetic Study

The Cibacron Brilliant Yellow 3G-P (CB) dye was used as an organic pollutant to examine the photocatalytic activity of Au-CuO-ZnO under visible light irradiation. Figure (11) shows the UV/Vis absorption spectra of (CB) dye solutions on Au-CuO-ZnO NPs when exposed to visible light over time. The results showed that as the irradiation period increased, the intensity of the UV-Vis absorption spectra for (CB) dye decreased. The drop in absorbance is attributed to a decrease in the concentration which might be attributable to the photodegradation of the dye chromogen, implying that the conjugated xanthene ring in (CB) dye is efficiently degraded by a catalyst. No additional absorption peaks were seen after 50 minutes of irradiation, indicating that the dye had fully mineralized. The photocatalytic performance of Au-CuO-ZnO photocatalyst was investigated as a pseudo-first-order kinetic model (equation 3), as shown in Figure (11), which shows a linear relationship between ln $C_o/C$ and irradiation time, supporting the conclusion that the photodegradation of dye obeys the pseudo-first-order kinetic model, which is consistent with previous studies on other organic dyes. In addition,
for (CB) dye photodegradation over Au-CuO-ZnO photocatalysts [31]. the pseudo-first-order kinetic constant was 1.67x10–3 $s^{-1}$.

$$\ln\left(\frac{C_0}{C_t}\right) = kt \qquad 3$$

## Recycling of photocatalyst

Photocatalyst stability and reusability have a significant impact on a variety of environmental applications; hence, photo/chemical stability is one of the key benefits of photocatalysts in a variety of applications. Five-cycle degradation experiments of (CB) dye were carried out under identical reaction conditions, except for changing the (CB) dye solution after each cycle, and without any washing or drying treatments of catalyst particles between successive runs, to investigate the photostability and reusability of the green synthesized Au-CuO-ZnO nanocomposite. Figure (12) indicates that after three runs, there is a modest decrease in the catalytic activity of the Au-CuO-ZnO nanocomposite. As a result, the photodegradation rate in the first reuse was 99.4%, the rate of photodegradation after the second use reuse is 92.6%, and the rate of photodegradation after the third is 87.9%, however, after four successive

cycles, the photocatalytic activity of the catalyst is over 87.6% of its initial value, confirming the photostability of the Au-CuO-ZnO nanocomposite and demonstrating the photocatalyst's reusability in the destruction of (CB) dye in aqueous solution. The photodegradation efficiency fell to 78.6 percent after only five cycles. Because the active sites of catalyst are filled by dye molecules and reaction intermediates, the drop in photodegradation efficiency might be ascribed to a decrease in catalyst surface area, Agglomeration of particles at high concentrations, in addition to adsorptive occupancy of active sites, may block the active sites of the catalyst, lowering photodegradation efficiency [32].

## Effect of Radical Scavengers

It is well known that the surface reactions are dominated by two primary reactive oxygen species: hydroxyl radicals $^{\bullet}OH$ and superoxide radicals $O_2^{\bullet-}$. Hydroxyl radicals are highly reactive, very powerful, and non-selective entities that attack and destroy most organic compounds in aqueous media, these species are the primary active agents in photodegradation, and increasing the rate of mineralization necessitates raising the concentration of this oxidizing agent, several scavengers can be used to explore the functions of these species in the photodegradation processes. Several scavengers were evaluated in this work, including para-benzoquinone for $O_2^{\bullet-}$ scavengers, potassium iodide for both $h^+$ and $^{\bullet}OH$ scavengers, and tert-butanol for $^{\bullet}OH$ scavengers, Figure (13) shows the influence of ROS on the photo decolorization percent of (CB) dye; after 120 minutes of irradiation, the photo decolorization efficiency of (CB) dye is 99.4 percent without scavenger. Under the same working conditions, when tert-butanol was added, the photo decolorization efficiency dropped to 37.1%, and when para-benzoquinone was added, the efficiency dropped to 62.3%. The addition of KI, on the other hand, resulted in an 18.6% reduction in photo decolorization efficiency, which might be attributed to the efficacy of Iodide ions, which are good scavengers that prevent valence band holes and adsorbed $^{\bullet}OH$ radicals, The predominant species are $^{\bullet}OH$ radicals, while the secondary species are $O_2^{\bullet-}$ radicals, according to these findings. Catalyst amount 1.0 g/L was used in all tests [33].

## Anticancer activity of Au-CuO-ZnO nanocomposite

The ability of Au-CuO-ZnO nanocomposite to kill and inhibit the growth of cancer cells was confirmed by measuring cytotoxicity, as an (MTT assay) test was carried out. (6.25,12.5 ,25,50,100) mcg/ml for 72 hours, as shown in Figure (14). Where the Au-CuO-ZnO nanocomposite showed high lethal effectiveness of cancer cells by inhibiting the growth and proliferation of cancer cells when compared to cancer cells not treated with the compound. The mechanism used by the Au-CuO-ZnO nanocomposite to kill cancer cells was also investigated, as the treated and untreated cancer cells were dyed with Thiazolyl Tetrazolium Methyl bromide dye, MTT measurement results for infected cells and healthy cells that were treated with tetrazolium salt of yellow color, which turns purple. The reason for the color change is due to the reduction of formazan by the enzyme Oxo reductase in the mitochondria, and the higher the number of living cells, the higher the absorption value of the compound under ultraviolet violet at a wavelength (570) nm UV. The process of measuring the toxicity of the prepared compounds is one of the most

important methods for detecting inhibition in living cells. The biological activity of Au-CuO-ZnO nanocomposite was: IC50=35.33 µg/ml [34,35].

## Antibacterial

The effect of Au-CuO-ZnO nanocomposite Prepared in an environmentally friendly way using Acacia dealbata leaf extract on the pathogenic bacteria of coli Escherichia and Staphylococcus aureus, where these bacteria were used as a representative of the cream-negative bacteria and the positive bacteria respectively. The first class of bacteria used is Gram-negative bacteria of the type of Escherichia coli, as the results showed that sample No. (1,2) has high efficacy, with inhibition diameters of (32 and 30) mm respectively, it gave 100% complete inhibition of bacteria, and the percentage of inhibition in Au-CuO-ZnO nanocomposite solution was higher than the antibiotics used, and for samples No. (3, 4) It showed good efficacy. Its damping diameters reached (23 and 21) mm, respectively. As for sample No. (6,5), it showed average effectiveness of damping diameters of (7 and 9) mm respectively, as figure (15) shows the effect of the antibiotics used on the bacteria (Escherichia coli) .

As for the second class of pathogenic bacteria under study, which is Gram-positive bacteria of the type, Staphylococcus aureus, the results showed that sample No. (1,2) is highly efficient, with inhibition diameters of (35 and 32) mm respectively, it gave 100% complete inhibition of bacteria, and the percentage of inhibition in Au-CuO-ZnO nanocomposite solution was higher than the antibiotics used, and for samples No. (3,4). It showed good potency. The damping diameters were (30 and 26) mm, respectively. As for sample No. (6,5), the efficacy of average damping diameters is (9 and 20) mm, respectively, as shown in Figure (15). The results showed the rate of success in eliminating and destroying these bacteria and this is possible by using the nanoscale solution to eliminate bacteria [36,37].

Table (4): Effect of prepared Au-CuO-ZnO nanocomposite on pathogenic bacteria (Escherichia coli, Staphylococcus aureus)

| Nanocomposite | *sample* | *E. coli* | *D.numbered (mm)* | Staph. aureus | *D.numbered (mm)* |
|---|---|---|---|---|---|
| Au-CuO-ZnO | 1 | *+++* | *32* | *+++* | *35* |
| | 2 | *+++* | *30* | *+++* | *32* |
| | 3 | *++* | *23* | *+++* | *30* |
| | 4 | *++* | *21* | *++* | *26* |
| | 5 | *+* | *7* | *+* | *9* |
| | 6 | *+* | *9* | *++* | *20* |

## Mechanism for photodegradation of CB dye

Photoexcitation, charge carrier separation, migration, and surface redox reduction reactions are the major processes in the photocatalytic process. Due to the relatively broadband gap energy (3.3 eV), bare ZnO applications have been limited due to poor charge separation and low visible light absorption. To increase the photoactivity of ZnO NPs, modification/decoration of ZnO with noble metal Au and narrow band gap semiconductor CuO was carried out in the current study. The formation of electron-hole pairs takes occurs when visible light is emitted on the Au-CuO-ZnO catalyst. By acting as an electron sink/trap on the semiconductor, the Au metal prevents the recombination of electron-hole pairs. Because CuO band positions were higher than ZnO CB and VB, photogenerated electrons moved from CuO to ZnO and photogenerated holes moved from ZnO to CuO. In the valence band, holes oxidize absorbed hydroxide ions ($OH^-$) to $^{\bullet}OH$, whereas electrons in the conduction band may decrease $O_2$ adsorbed onto zinc-binding sites to create surface-bound superoxide radicals ($O_2^{\bullet-}$). Dyes are degraded by these extremely reactive radicals into non-toxic $CO_2$ and $H_2O$. It is necessary to explore which reactive radical species play a major role in the photocatalytic performance of Au-CuO-ZnO nanocomposite to suggest the (CB) dye photodegradation process over Au-CuO-ZnO photocatalyst. The $^{\bullet}OH$, $h^+$, and $O_2^{\bullet-}$ reactive species are suppressed during the photodegradation of Cibacron Brilliant Yellow 3G-P dye over Au-CuO- ZnO by adding tert-butanol (TB, $^{\bullet}OH$ trap), potassium iodide (KI, $^{\bullet}OH$ and $h^+$ trap), and para-benzoquinone (BQ, $O_2^{\bullet-}$ trap) to the reaction solution, respectively. The photodegradation efficiency in the presence and absence of scavengers is shown in Figure (11). The photodegradation efficiency of (CB) dye was only marginally influenced by the addition of TB and BQ. However, the results show that under visible light illumination, KI scavenger greatly reduced (CB) dye photodegradation over Au-CuO-ZnO, demonstrating that both $h^+$ and $^{\bullet}OH$ are involved in (CB) dye photodegradation.

$$ZnO + hv \rightarrow ZnO\ (h_{VB}^{+} + e_{CB}^{-}) \quad (4)$$

$$O_2 + e_{CB}^{-} \rightarrow O_2^{\bullet-} \quad (5)$$

$$OH^- + h_{VB}^{+} \rightarrow {}^{\bullet}OH \quad (6)$$

$$O_2^{\bullet-} + CB \rightarrow \text{dye degradation} \quad (7)$$

$$^{\bullet}OH + CB \rightarrow \text{dye degradation} \quad (8)$$

$$CB + h_{VB}^{+} \rightarrow \text{dye degradation} \quad (9)$$

# Conclusions

In conclusion, a simple green technique was used to produce ZnO, CuO, Au, CuO-ZnO, Au-ZnO, and Au-CuO-ZnO NPs. XRD, FE-SEM, EDX, TEM, and AFM, methods were used to examine the Aspects of nanomaterials as-prepared that are structural, morphological, optical, elemental, topographical, and chemical. The photodegradation efficiency rose from 54.6 percent (bare ZnO) to 99.4 percent (doped

ZnO) as the absorption peak of ZnO was pushed towards the visible range by doping ZnO with Au and CuO. (Au-CuO-ZnO). Under visible light irradiation, the Au-CuO-ZnO nanocomposite demonstrated its potential as a photocatalyst for (CB) dye degradation. Long-term irradiation, A higher photocatalyst loading of up to 1.0 g/L and a lower starting dye concentration, the photodegradation efficiency of (CB) dye increased in general. Degradation is more efficient in a basic media than in an acidic medium. and study the Effect of prepared Au-CuO-ZnO nanocomposite on pathogenic bacteria (Escherichia coli, Staphylococcus aureus). It was shown that Au-CuO-ZnO nanocomposite has the ability to kill cancer cells and inhibit their proliferation through the evaluation of cytotoxicity. The Au-CuO-ZnO nanocomposite displayed remarkable lethal efficacy against cancer cells by halting their development and multiplication, in contrast to untreated cancer cells. The biological activity of the Au-CuO-ZnO nanocomposite has an IC50 of 35.33 g/ml.

# Declarations


### Acknowledgments

The authors express their thankfulness to the Al-Mustaqbal University College for the support provided to accomplish this study.


### Ethical Approval

Not applicable

### Competing interests

The authors declare there are no competing of interests

### Authors' contributions

1,2 and 3 Experimental part

4 and 5 wrote the main manuscript text

6 and prepared figures

7,8 and 9 proofreading

All authors reviewed the manuscript.


### Funding

There are no funding for this work


### Availability of data and materials

Not applicable

# References


1. Laxmi, V., & Kaushik, G. (2020). Toxicity of hexavalent chromium in environment, health threats, and its bioremediation and detoxification from tannery wastewater for environmental safety. In *Bioremediation of industrial waste for environmental safety* (pp. 223-243). Springer, Singapore.
2. Velusamy, S., Roy, A., Sundaram, S., & Kumar Mallick, T. (2021). A review on heavy metal ions and containing dyes removal through graphene oxide-based adsorption strategies for textile wastewater treatment. *The Chemical Record*, *21*(7), 1570-1610.
3. Al-Tohamy, R., Ali, S. S., Li, F., Okasha, K. M., Mahmoud, Y. A. G., Elsamahy, T., ... & Sun, J. (2022). A critical review on the treatment of dye-containing wastewater: Ecotoxicological and health concerns of textile dyes and possible remediation approaches for environmental safety. *Ecotoxicology and Environmental Safety*, *231*, 113160.
4. Lu, Z. Y., Ma, Y. L., Zhang, J. T., Fan, N. S., Huang, B. C., & Jin, R. C. (2020). A critical review of antibiotic removal strategies: Performance and mechanisms. *Journal of Water Process Engineering*, *38*, 101681.
5. Khan, S., Naushad, M., Al-Gheethi, A., & Iqbal, J. (2021). Engineered nanoparticles for removal of pollutants from wastewater: Current status and future prospects of nanotechnology for remediation strategies. *Journal of Environmental Chemical Engineering*, *9*(5), 106160.
6. Hazim, K., Khudair, Z. F., Kadhim, I. K., Mohamed, L., Hameed, G. F., & Alyasiri, F. J. (2022). Biosynthesis, Antibacterial Activity, The Photocatalytic Performance of ZNO NPS by use of Leaf Extract of the Plant Primo Fiore. *Pakistan Journal of Medical & Health Sciences*, *16*(04), 456-456.
7. Raizada, P., Sudhaik, A., & Singh, P. (2019). Photocatalytic water decontamination using graphene and ZnO coupled photocatalysts: a review. *Materials Science for Energy Technologies*, *2*(3), 509-525.
8. Karthikeyan, C., Arunachalam, P., Ramachandran, K., Al-Mayouf, A. M., & Karuppuchamy, S. (2020). Recent advances in semiconductor metal oxides with enhanced methods for solar photocatalytic applications. *Journal of Alloys and Compounds*, *828*, 154281.
9. Koppala, S., Xia, Y., Zhang, L., Peng, J., Chen, Z., & Xu, L. (2019). Hierarchical ZnO/Ag nanocomposites for plasmon-enhanced visible-light photocatalytic performance. *Ceramics International*, *45*(12), 15116-15121.
10. Asemi, M., Ahmadi, M., & Ghanaatshoar, M. (2018). Preparation of highly conducting Al-doped ZnO target by vacuum heat-treatment for thin film solar cell applications. *Ceramics International*, *44*(11), 12862-12868.
11. Fouda, A., Salem, S. S., Wassel, A. R., Hamza, M. F., & Shaheen, T. I. (2020). Optimization of green biosynthesized visible light active CuO/ZnO nano-photocatalysts for the degradation of organic methylene blue dye. *Heliyon*, *6*(9), e04896.

12. Thakur, A., Sharma, N., Bhatti, M., Sharma, M., Trukhanov, A. V., Trukhanov, S. V., ... & Thakur, P. (2020). Synthesis of barium ferrite nanoparticles using rhizome extract of Acorus calamus: characterization and its efficacy against different plant phytopathogenic fungi. *Nano-Structures & Nano-Objects*, *24*, 100599.
13. Hazim, K., Hamza, Z., & Mohamed, L. (2022). Eco-Friendly Synthesis, Antibacterial Activity, and Photocatalytic Performance of ZnO Nanoparticles Synthesized via Leaves Extract of Paraserianthes Lophantha. *Pakistan Journal of Medical & Health Sciences*, *16*(03), 581-581.
14. Lee, Y. J., Song, K., Cha, S. H., Cho, S., Kim, Y. S., & Park, Y. (2019). Sesquiterpenoids from Tussilago farfara flower bud extract for the eco-friendly synthesis of silver and gold nanoparticles possessing antibacterial and anticancer activities. *Nanomaterials*, *9*(6), 819.
15. Sharma, S., Kumar, K., Thakur, N., Chauhan, S., & Chauhan, M. S. (2021). Eco-friendly Ocimum tenuiflorum green route synthesis of CuO nanoparticles: Characterizations on photocatalytic and antibacterial activities. *Journal of Environmental Chemical Engineering*, *9*(4), 105395.
16. Ahmad, M., Rehman, W., Khan, M. M., Qureshi, M. T., Gul, A., Haq, S., ... & Menaa, F. (2021). Phytogenic fabrication of ZnO and gold decorated ZnO nanoparticles for photocatalytic degradation of Rhodamine B. *Journal of Environmental Chemical Engineering*, *9*(1), 104725.
17. Lai, Y. S., Cheng, C. T., Liou, J. L., Jehng, J. M., & Dai, Y. M. (2021). The ZnO–Au-Titanium oxide nanotubes (TiNTs) composites photocatalysts for CO2 reduction application. *Ceramics International*, *47*(21), 30020-30029.
18. Alavi, M., Dehestaniathar, S., Mohammadi, S., Maleki, A., & Karimi, N. (2021). Antibacterial activities of phytofabricated ZnO and CuO NPs by Mentha pulegium leaf/flower mixture extract against antibiotic resistant bacteria. *Advanced Pharmaceutical Bulletin*, *11*(3), 497.
19. Kant, R., Pathak, S., & Dutta, V. (2018). Design and fabrication of sandwich-structured α-Fe2O3/Au/ZnO photoanode for photoelectrochemical water splitting. *Solar Energy Materials and Solar Cells*, *178*, 38-45.
20. Liu, T., Zhao, Q., Xie, Y., Jiang, D., Chu, Z., & Jin, W. (2020). In situ fabrication of aloe-like Au–ZnO micro/nanoarrays for ultrasensitive biosensing of catechol. *Biosensors and Bioelectronics*, *156*, 112145.
21. Ouarez, L., Chelouche, A., Touam, T., Mahiou, R., Djouadi, D., & Potdevin, A. (2018). Au-doped ZnO sol-gel thin films: an experimental investigation on physical and photoluminescence properties. *Journal of Luminescence*, *203*, 222-229.
22. Pandiyan, N., Murugesan, B., Arumugam, M., Sonamuthu, J., Samayanan, S., & Mahalingam, S. (2019). Ionic liquid-a greener templating agent with Justicia adhatoda plant extract assisted green synthesis of morphologically improved Ag-Au/ZnO nanostructure and it's antibacterial and anticancer activities. *Journal of Photochemistry and Photobiology B: Biology*, *198*, 111559.
23. Dobrucka, R. (2021). Facile synthesis of trimetallic nanoparticles Au/CuO/ZnO using Vitex agnus-castus extract and their activity in degradation of organic dyes. *International Journal of Environmental Analytical Chemistry*, *101*(14), 2046-2057.

24. Wentao, W., Tao, Z., Bulei, S., Tongchang, Z., Qicheng, Z., Fan, W., ... & Yi, S. (2019). Functionalization of polyvinyl alcohol composite film wrapped in am-ZnO@ CuO@ Au nanoparticles for antibacterial application and wound healing. *Applied Materials Today*, *17*, 36-44.
25. Dobrucka, R., Kaczmarek, M., Łagiedo, M., Kielan, A., & Dlugaszewska, J. (2019). Evaluation of biologically synthesized Au-CuO and CuO-ZnO nanoparticles against glioma cells and microorganisms. *Saudi Pharmaceutical Journal*, *27*(3), 373-383.
26. Nasrollahi, N., Vatanpour, V., Aber, S., & Mahmoodi, N. M. (2018). Preparation and characterization of a novel polyethersulfone (PES) ultrafiltration membrane modified with a CuO/ZnO nanocomposite to improve permeability and antifouling properties. *Separation and Purification Technology*, *192*, 369-382.
27. Singh, J., & Soni, R. K. (2021). Efficient charge separation in Ag nanoparticles functionalized ZnO nanoflakes/CuO nanoflowers hybrids for improved photocatalytic and SERS activity. *Colloids and Surfaces A: Physicochemical and Engineering Aspects*, *626*, 127005.
28. Chen, J., Gu, A., Miensah, E. D., Liu, Y., Wang, P., Mao, P., ... & Yang, Y. (2021). Core-shell ZnO@ Cu2O encapsulated Ag NPs nanocomposites for photooxidation-adsorption of iodide anions under visible light. *Separation and Purification Technology*, *262*, 118328.
29. Singh, J., & Soni, R. K. (2020). Controlled synthesis of CuO decorated defect enriched ZnO nanoflakes for improved sunlight-induced photocatalytic degradation of organic pollutants. *Applied Surface Science*, *521*, 146420.
30. Raizada, P., Sudhaik, A., Patial, S., Hasija, V., Khan, A. A. P., Singh, P., ... & Nguyen, V. H. (2020). Engineering nanostructures of CuO-based photocatalysts for water treatment: current progress and future challenges. *Arabian Journal of Chemistry*, *13*(11), 8424-8457.
31. Nadargi, D. Y., Tamboli, M. S., Patil, S. S., Dateer, R. B., Mulla, I. S., Choi, H., & Suryavanshi, S. S. (2020). Microwave-epoxide-assisted hydrothermal synthesis of the CuO/ZnO heterojunction: a highly versatile route to develop H2S gas sensors. *ACS omega*, *5*(15), 8587-8595.
32. Singh, J., & Soni, R. K. (2021). Efficient charge separation in Ag nanoparticles functionalized ZnO nanoflakes/CuO nanoflowers hybrids for improved photocatalytic and SERS activity. *Colloids and Surfaces A: Physicochemical and Engineering Aspects*, *626*, 127005.
33. Kaur, A., Anderson, W. A., Tanvir, S., & Kansal, S. K. (2019). Solar light active silver/iron oxide/zinc oxide heterostructure for photodegradation of ciprofloxacin, transformation products and antibacterial activity. *Journal of colloid and interface science*, *557*, 236-253.
34. Dobrucka, R., Romaniuk-Drapała, A., & Kaczmarek, M. (2021). Anti-leukemia activity of Au/CuO/ZnO nanoparticles synthesized used verbena officinalis extract. *Journal of Inorganic and Organometallic Polymers and Materials*, *31*(1), 191-202.
35. Zadeh, F. A., Bokov, D. O., Salahdin, O. D., Abdelbasset, W. K., Jawad, M. A., Kadhim, M. M., ... & Khatami, M. (2022). Cytotoxicity evaluation of environmentally friendly synthesis Copper/Zinc bimetallic nanoparticles on MCF-7 cancer cells. *Rendiconti Lincei. Scienze Fisiche e Naturali*, 1-7.

36. Juneja, S., Madhavan, A. A., Ghosal, A., Moulick, R. G., & Bhattacharya, J. (2018). Synthesis of graphenized Au/ZnO plasmonic nanocomposites for simultaneous sunlight mediated photo-catalysis and anti-microbial activity. *Journal of Hazardous Materials*, *347*, 378-389.
37. He, X., Yang, D. P., Zhang, X., Liu, M., Kang, Z., Lin, C., ... & Luque, R. (2019). Waste eggshell membrane-templated CuO-ZnO nanocomposites with enhanced adsorption, catalysis and antibacterial properties for water purification. *Chemical Engineering Journal*, *369*, 621-633.

# Figures

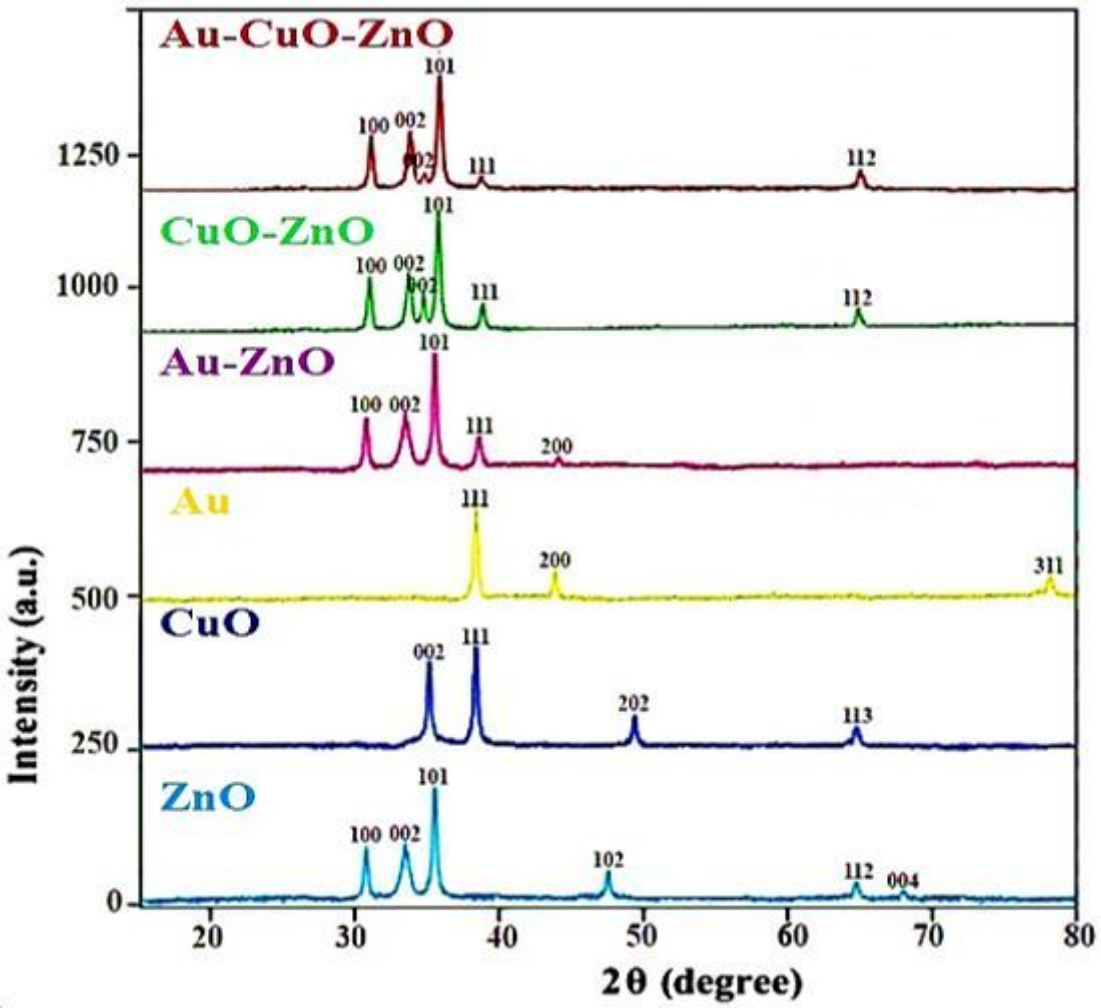


**Figure 1**

XRD of CuO, ZnO, Au, CuO-ZnO and Au-ZnO and Au-CuO-ZnO

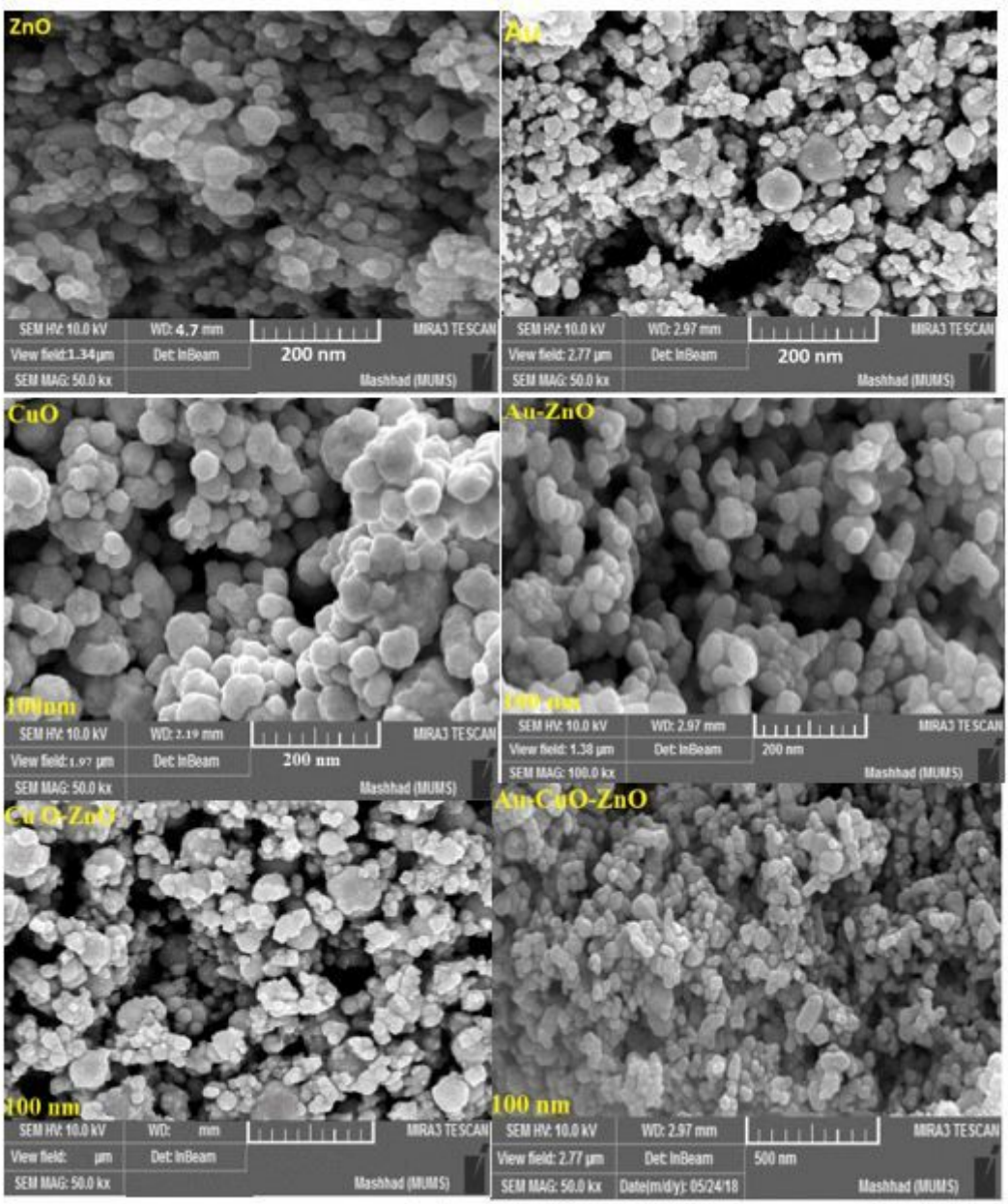


## Figure 2

FE-SEM Images of the ZnO, Au, CuO,Au-ZnO, Cu O-ZnO, Au-CuO-ZnO

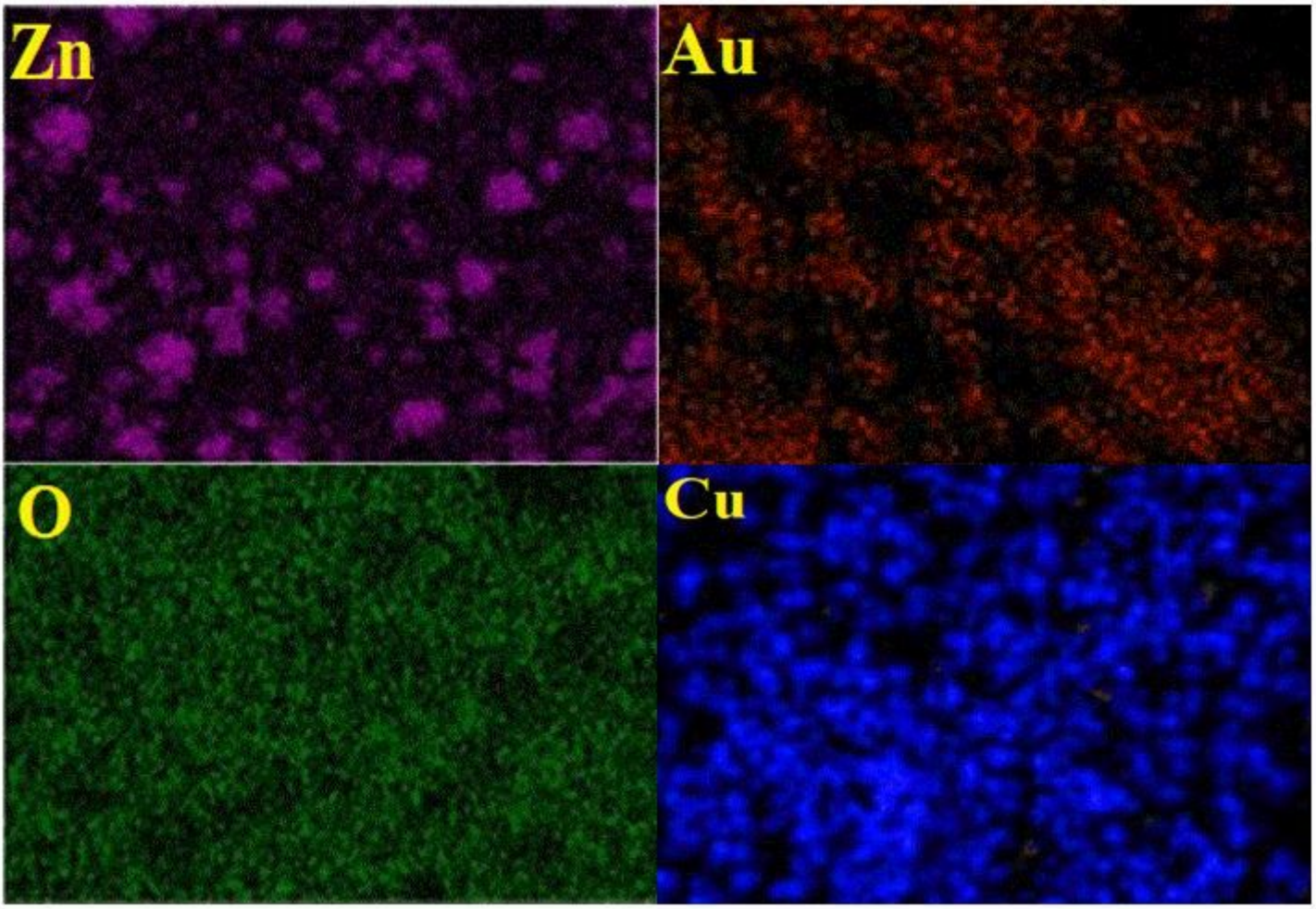


## Figure 3

Images representing the elements Zinc, Copper, Gold, and Oxygen for the prepared nanocomposite

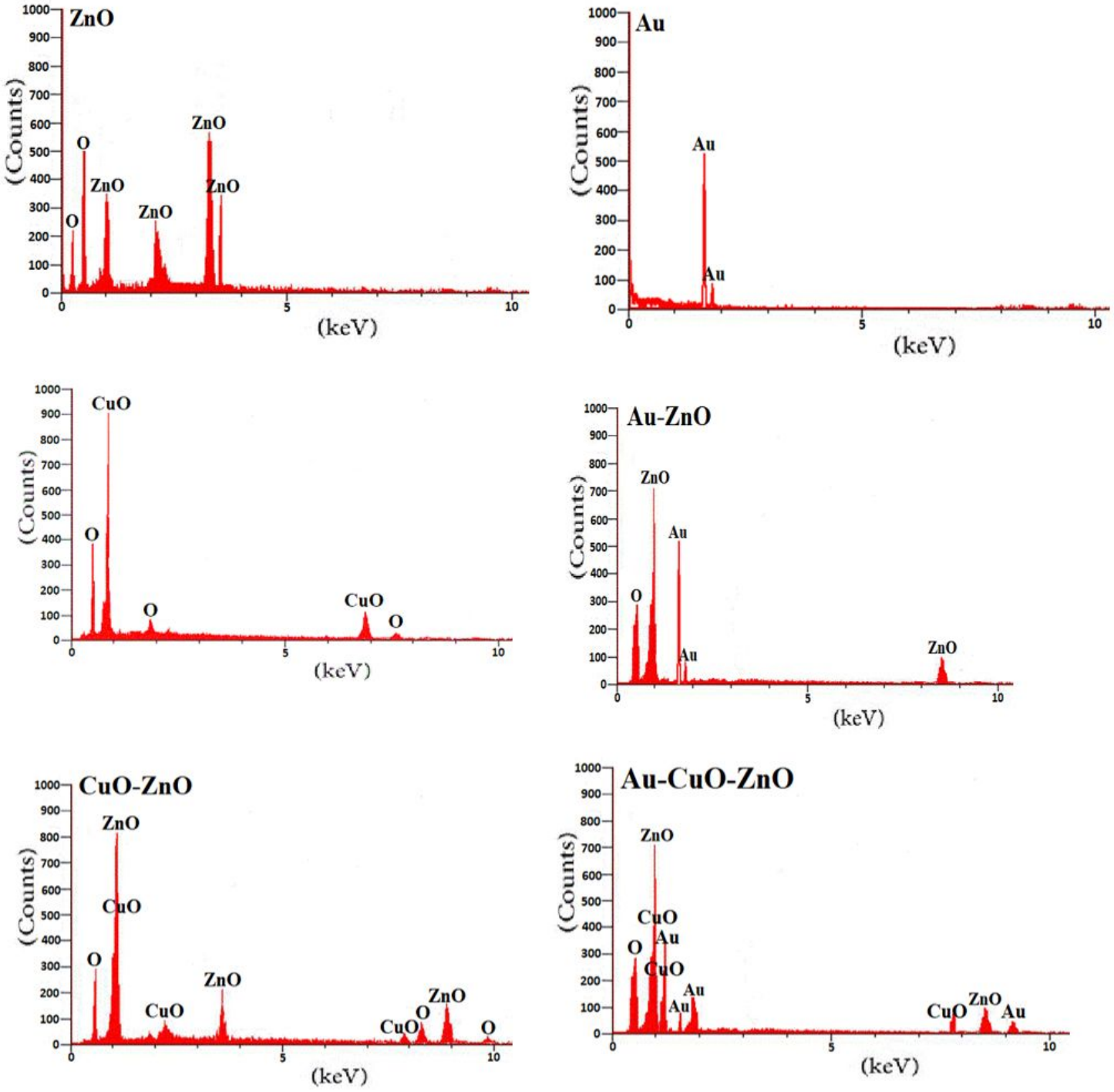


## Figure 4

EDX for the ZnO, Au, CuO, Au-ZnO and CuO-ZnO and Au-CuO-ZnO

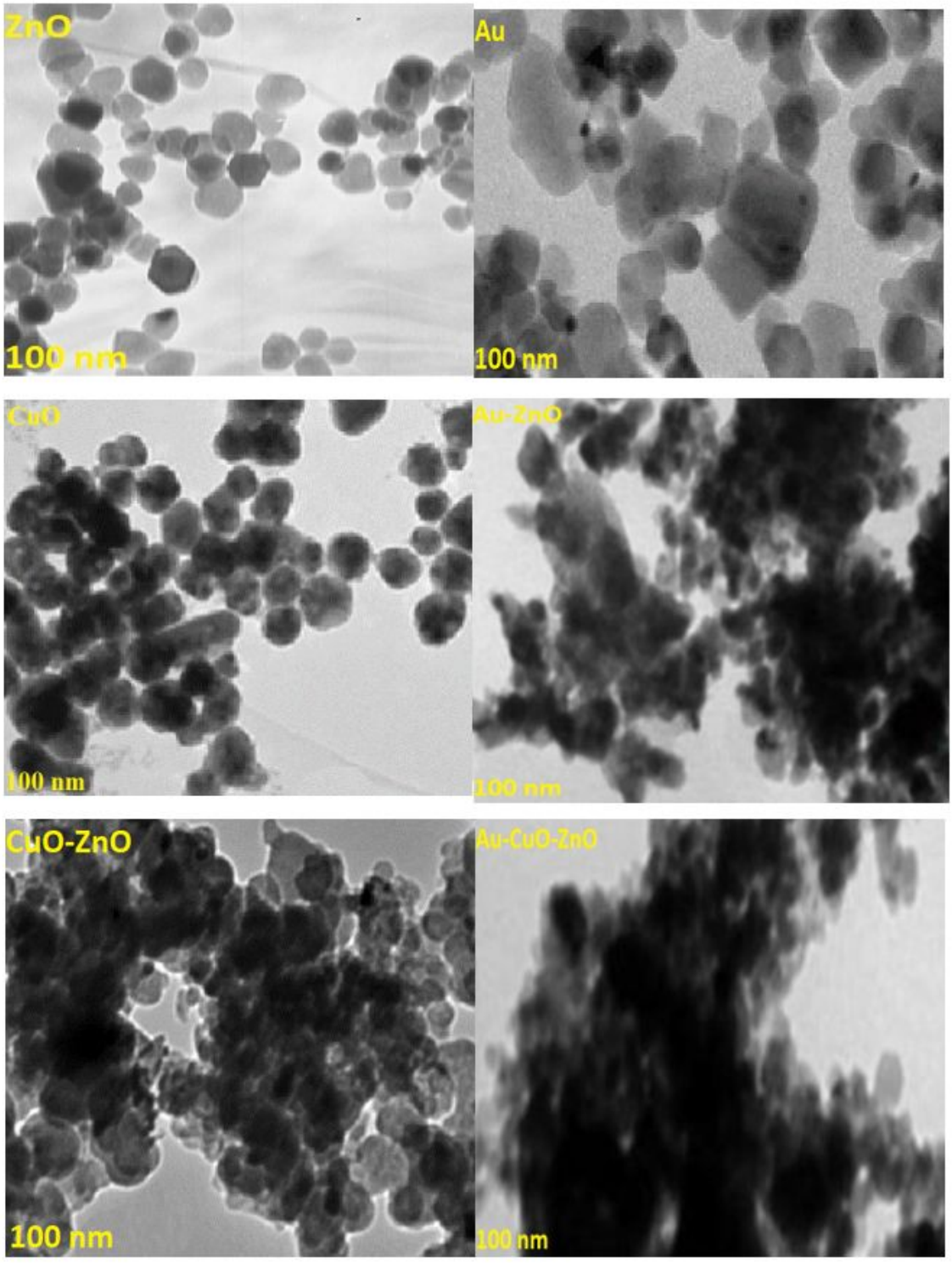


## Figure 5

TEM images of ZnO, Au, CuO, Au-ZnO, CuO-ZnO, Au-CuO-ZnO nanocomposite

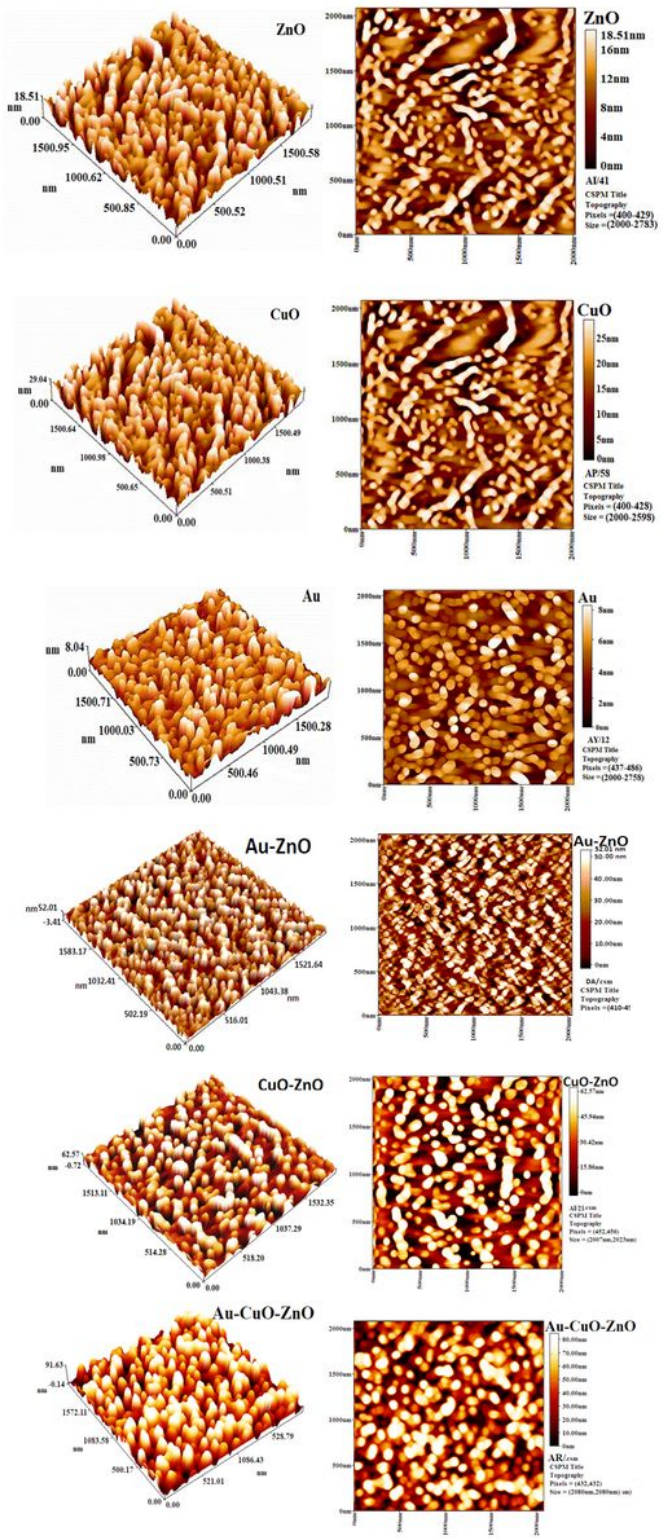


## Figure 6

3D and 2D image of AFM for of ZnO, Au, CuO, Au-ZnO, CuO-ZnO, Au-CuO-ZnO nanocomposite

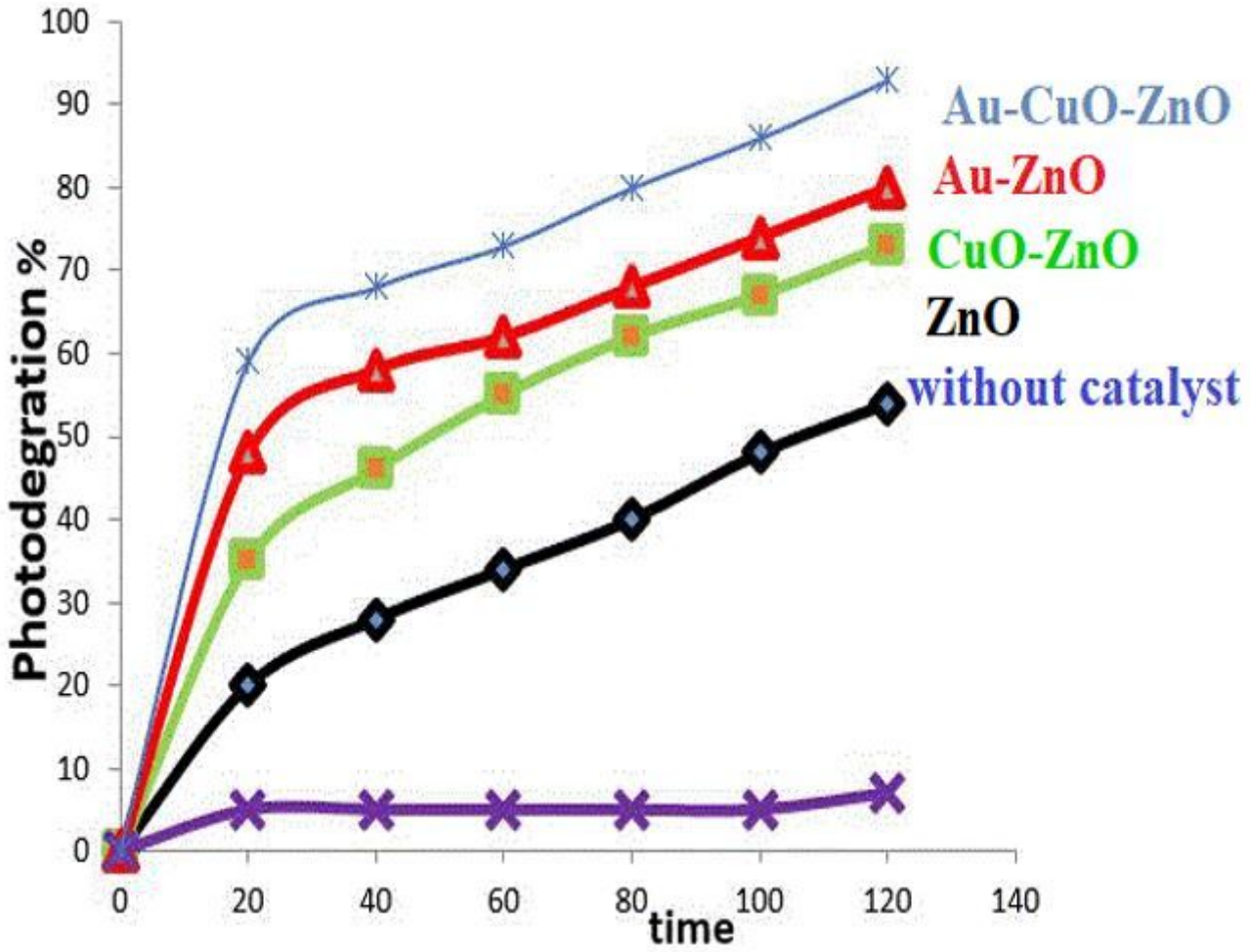


Figure 7

represents the efficiency of the optical degradation process of the Cibacron Brilliant Yellow 3G-P dye in the presence of nanomaterials

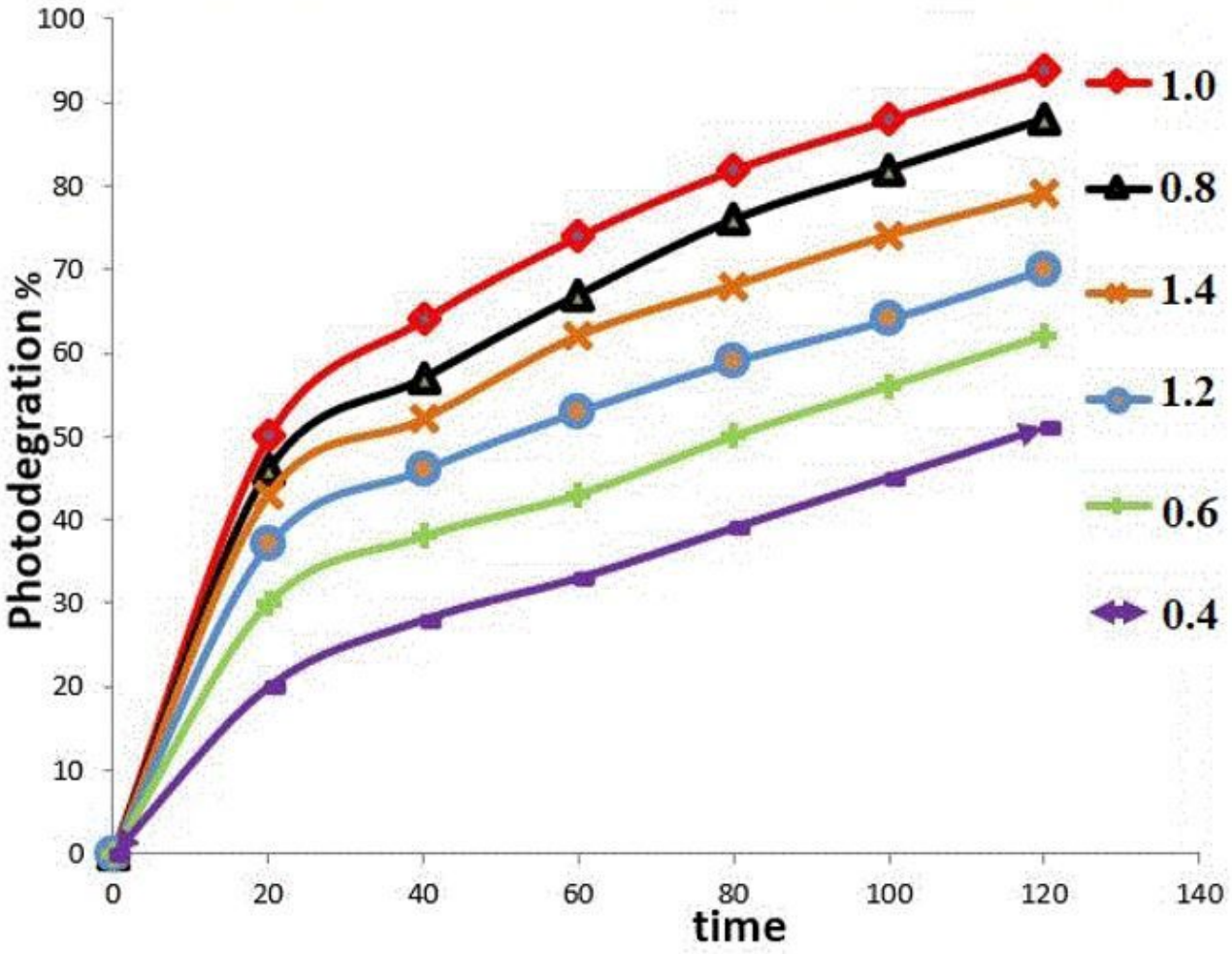


**Figure 8**

the catalytic activity of various photocatalysts

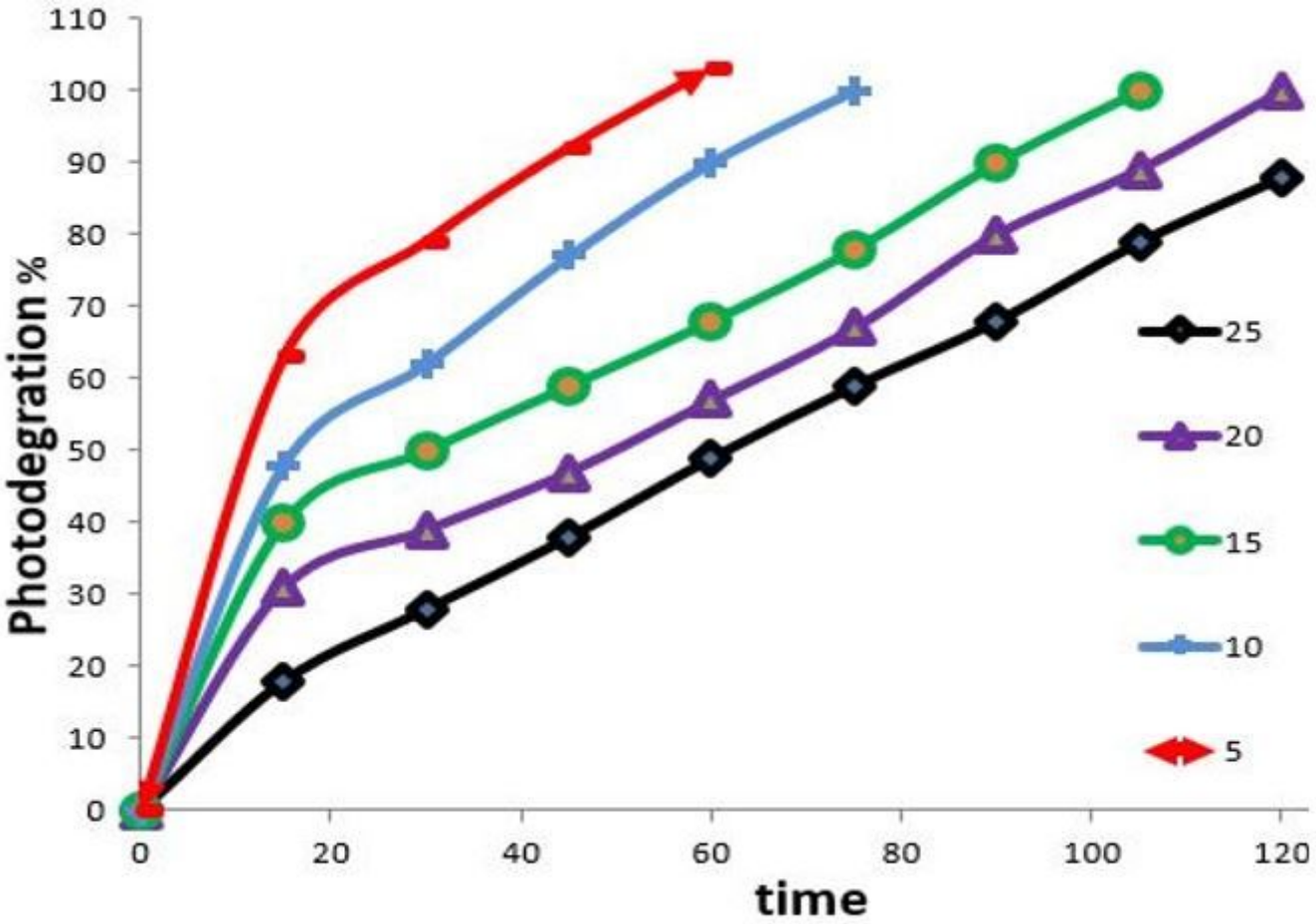


**Figure 9**

The effect of dye concentration on the photocatalytic photodegradation process

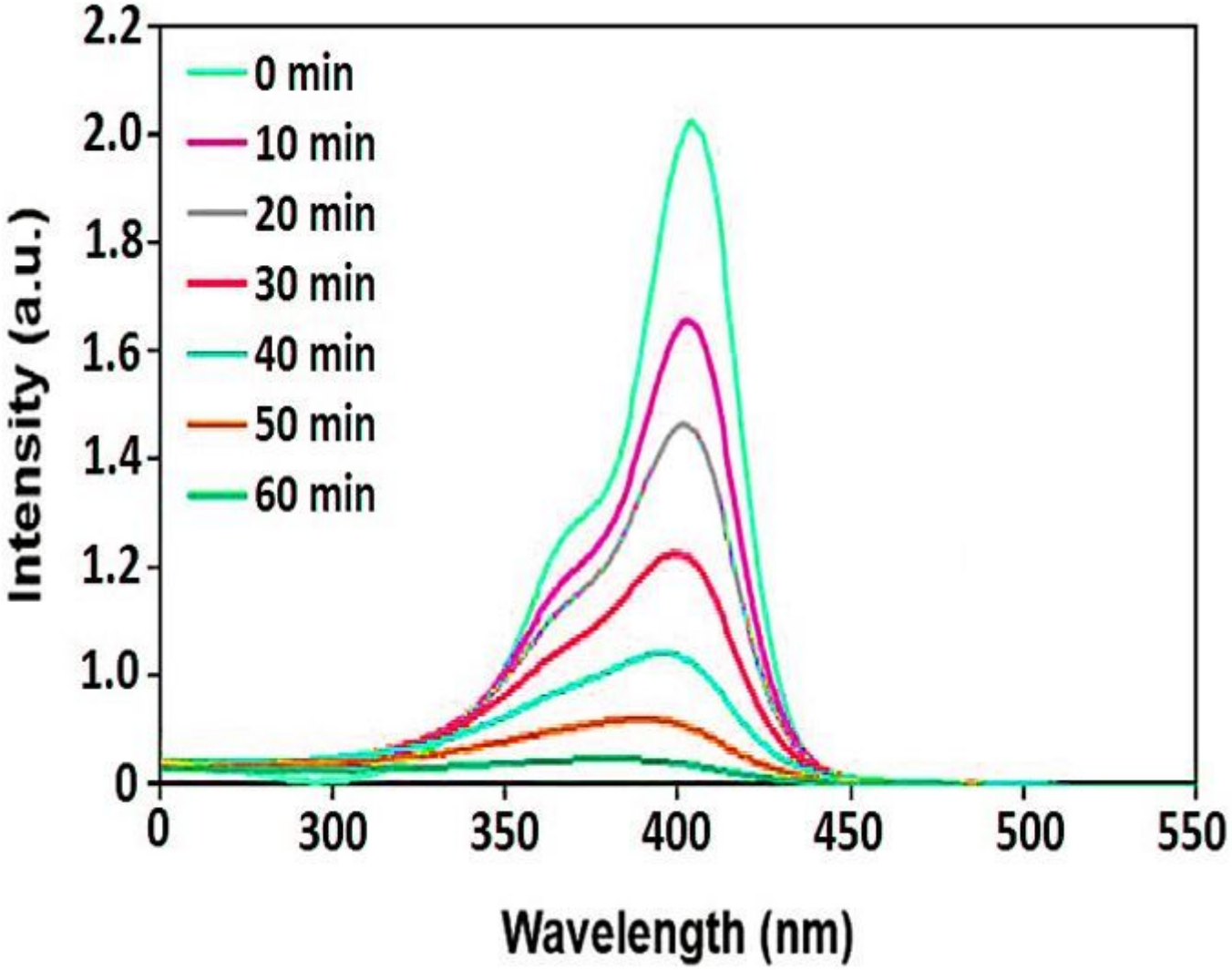


**Figure 10**

Effect of pH solution on the degradation of Cibacron Brilliant Yellow 3G-P (CB) dye

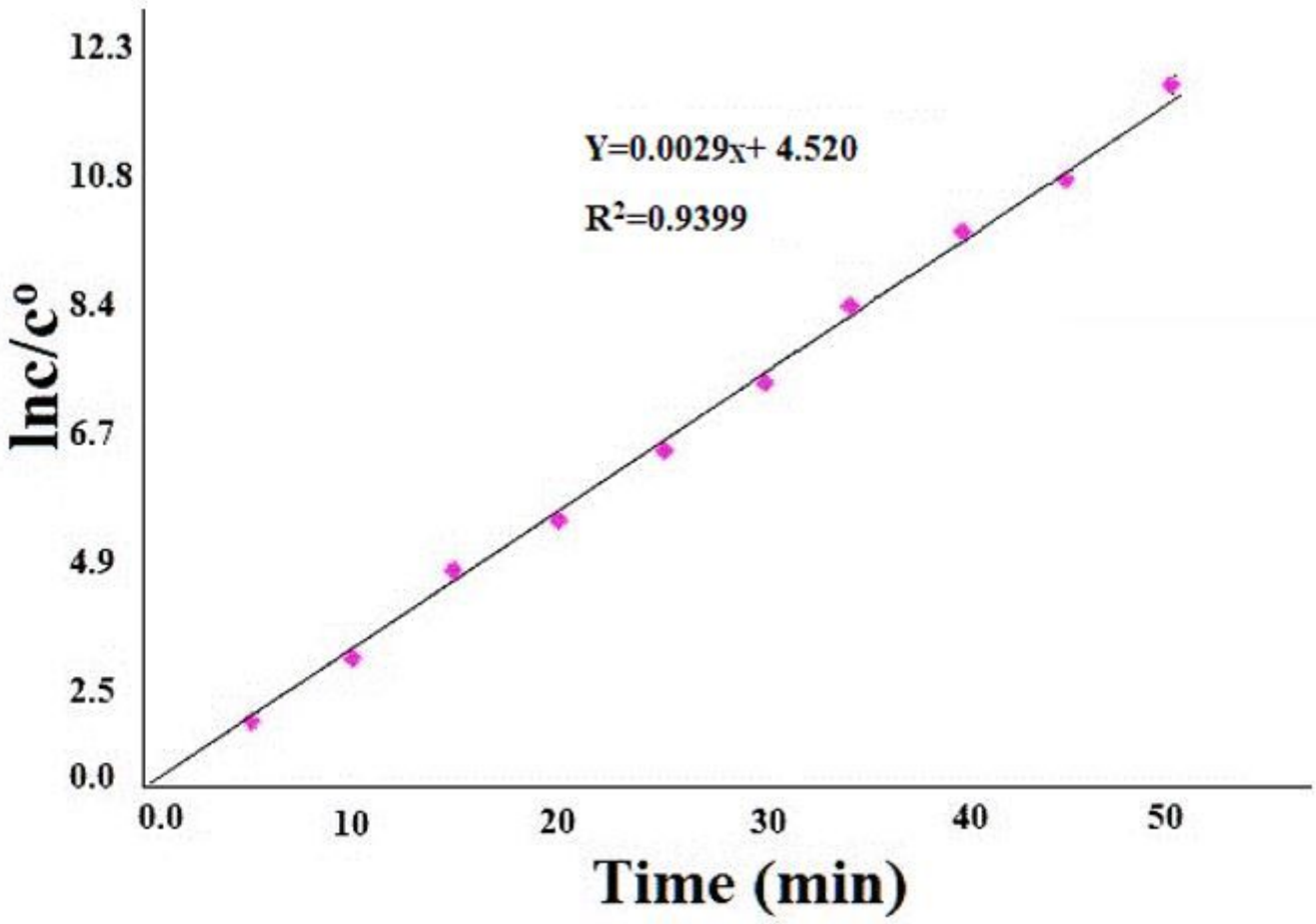


## Figure 11

Pseudo-first order kinetics for degradation (CB) dye and Au-CuO-ZnO

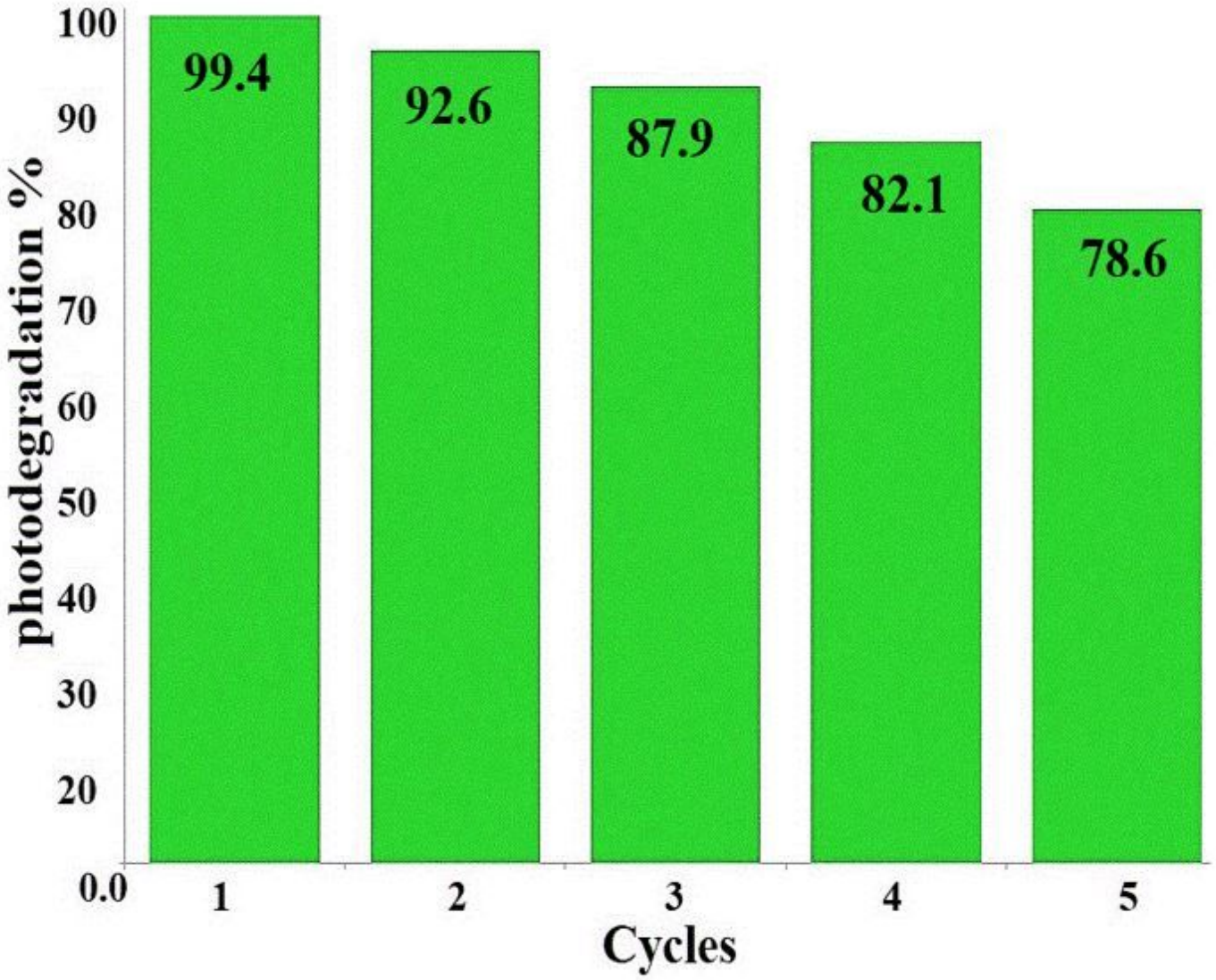


**Figure 12**

represents the reuse of the Au-CuO-ZnO

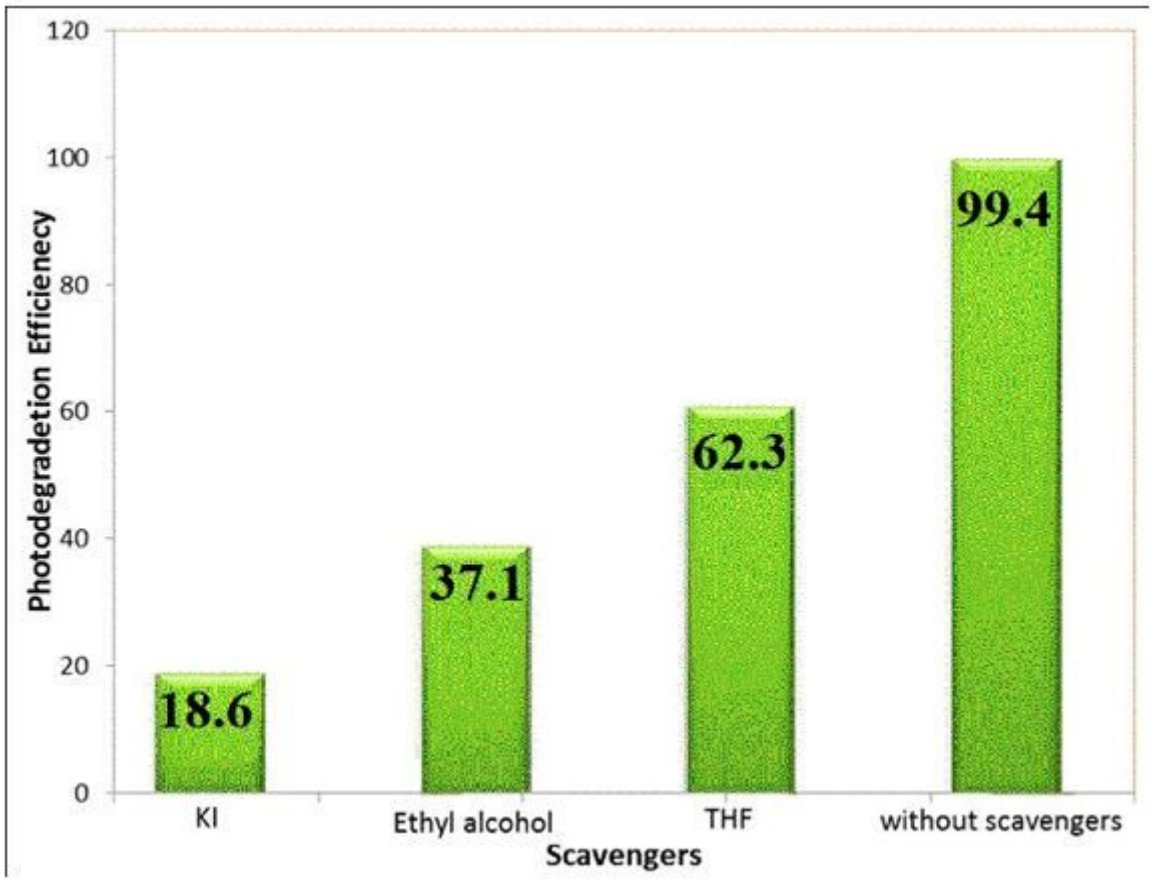


Figure 13

represents the reuse of the catalyst Au-CuO-ZnO nanocomposite

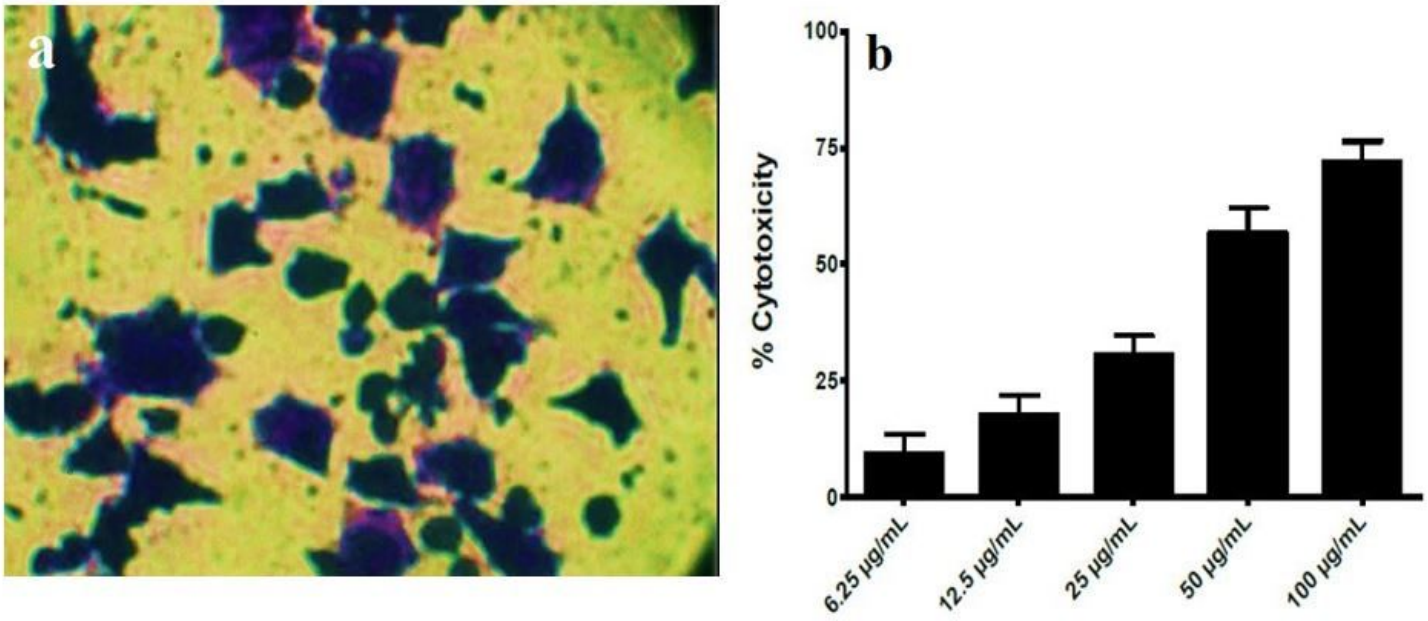


Figure 14

(a): on breast cancer cells MCF-7 (b): represents the effect ofAu-CuO-ZnO nanocomposite on breast cancer cells IC50,35.33.

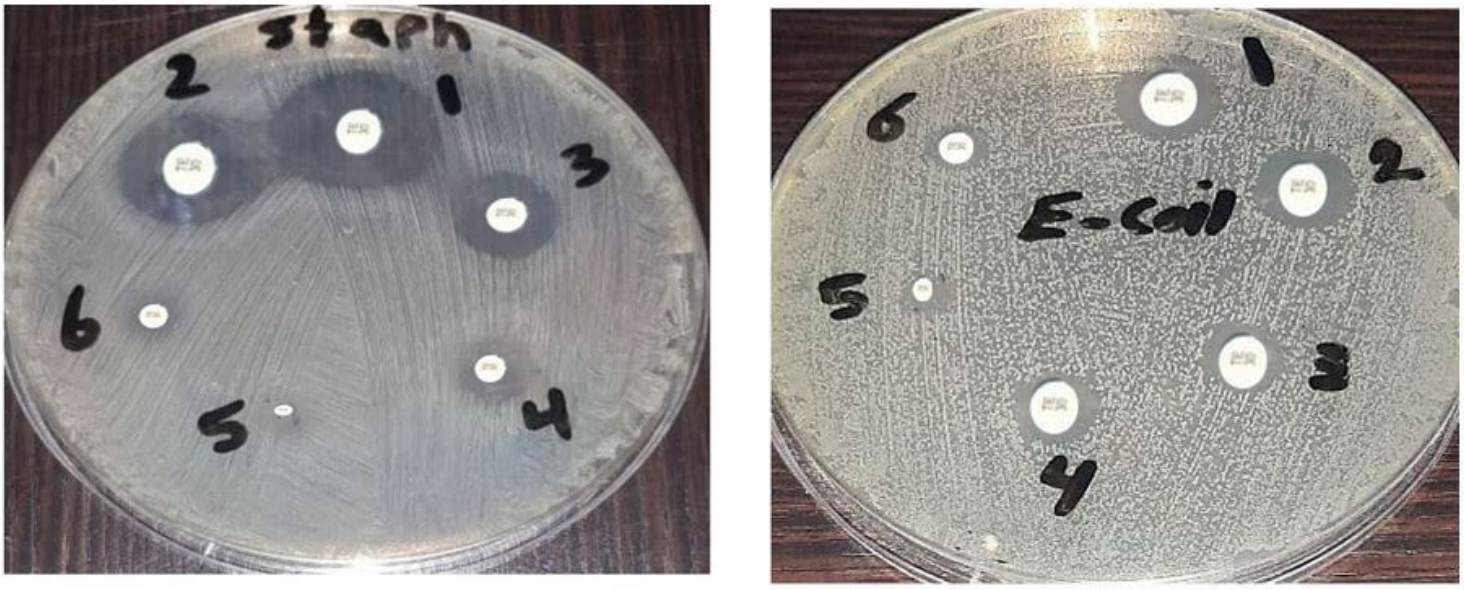


**Figure 15**

Effect of prepared Au-CuO-ZnO nanocomposite on pathogenic bacteria (E-coli, S-aureus)